The cellular landscape of the endochondral bone during the transition to extrauterine life.

Alejandro Díaz Rueda[1,4], Irepan Salvador-Martínez[2,4], Ismael Sospedra-Arrufat[1], Ana Alcaina-Caro[1], Ana Fernández-Miñán[1], Ana M. Burgos-Ruiz[1], Ildefonso Cases[1], Alberto Mohedano[3], Juan J. Tena[1], Holger Heyn[2], Javier Lopez-Rios[1,*], and Gretel Nusspaumer[1,*]

[1]Centro Andaluz de Biología del Desarrollo (CABD), CSIC-Universidad Pablo de Olavide-Junta de Andalucía, 41013 Seville, Spain.

[2]CNAG-CRG, Centre for Genomic Regulation (CRG), Barcelona Institute of Science and Technology (BIST), 08028 Barcelona, Spain.

[3]Intensive Care Unit, Severo Ochoa University Hospital Leganés, 28911 Madrid, Spain.

[4]These authors contributed equally

*Correspondence: javier.lopez-rios@csic.es, gnusda@upo.es

Running title: A single cell map of the perinatal bone

Keywords: mesenchymal stromal skeletal progenitors, endochondral ossification, fibroblast, scRNA-seq, mouse, birth.

Abstract

The cellular complexity of the endochondral bone underlies its essential and pleiotropic roles during organismal life. While the adult bone has received significant attention, we still lack a deep understanding of the perinatal bone cellulome. Here, we have profiled the full composition of the murine endochondral bone at the single-cell level during the transition from fetal to newborn life and in comparison to the adult tissue, with particular emphasis on the mesenchymal compartment. The perinatal bone contains different fibroblastic clusters with blastema-like characteristics in organizing and supporting skeletogenesis, angiogenesis, and hematopoiesis. Our data also suggests dynamic inter- and intra-compartment interactions as well as a bone marrow milieu that seems prone to anti-inflammation, which we hypothesize is necessary to ensure the proper program of lymphopoiesis and the establishment of central and peripheral tolerance in early life. Our study provides an integrative roadmap for the future design of genetic and cellular functional assays to validate cellular interactions and lineage relationships within the perinatal bone.

INTRODUCTION

Important changes take place during the transition from intrauterine to extrauterine life. The newborn is reaved of nutrients, heat and the buoyant and pathogen-protected environment of the womb. Among other large organismal changes, lungs are inflated and the cardiovascular flow adjusted as the newborn starts breathing. High hormonal levels are present in preparation for the sharp increase in the metabolic rate and thermoregulation. Brown fat tissue, accumulated during late gestation, plays an important metabolic and thermal role during the first days of life. Increased mechanical load and movement impacts on the skeleton of the newborn, where the osteogenic program will also be affected by the increase in oxygen supply. The establishment of the intestinal microbiome and its crosstalk with the still immature immune system will impact as well on the program of hematopoiesis in the bone marrow which started to build at late fetal stages (Hillman et al., 2012; Liggins, 1994; Morton and Brodsky, 2016; Sanidad and Zeng, 2020). The skeleton has a pivotal position in many of these processes, given its roles in body support, movement, organ protection, hematopoiesis and hormonal and metabolic control.

Endochondral bone-derived mesenchymal progenitors are able to engage in chondrogenic, osteogenic and adipogenic programs of differentiation, in addition to their specialization into bone marrow stromal cells (BMSC) that support hematopoiesis (Bianco and Robey, 2015). Development of long bones is a dynamic and tightly orchestrated process which reflects the capacity of mesenchymal progenitors to first generate cartilage, which will serve as a mold and will provide the signals to start the program of osteogenesis and the formation of the bone marrow (BM) (Galea et al., 2021; Haraguchi et al., 2019; Long and Ornitz, 2013). During the formation of the BM, some mesenchymal progenitors will stay as BMSC, supporting hematopoiesis, but will also hold the capacity to differentiate into osteoblasts and adipocytes (Comazzetto et al., 2021; Jeffery et al., 2022; Shu et al., 2021). Genetic cell-fate tracking, prospective immunophenotype characterization and, recently, scRNAseq studies in the mouse are revealing the complex nature of the bone mesenchymal compartment,

as well as the versatility of the different populations and their division of labor (Li et al., 2022a). For example, the capacity of hypertrophic chondrocytes to transdifferentiate into osteoblasts is now well accepted in the field (Hallett et al., 2021; Yang et al., 2014; Zhou et al., 2014). Moreover, bone fracture and fingertip regeneration mouse models, along with studies on limb regeneration in other vertebrates, are challenging ingrained concepts and pointing to alternative models by which different populations (e.g. fibroblastic cells) can be recruited and reprogrammed in a highly plastic fashion, which includes cellular phenotypic convergence (Jeffery et al., 2022; Johnson et al., 2020; Lin et al., 2021; Matsushita et al., 2021; Newton et al., 2019; Storer et al., 2020; Zhou et al., 2014). Most of these studies have nevertheless focused on the adult bone, and we still lack fundamental knowledge on the heterogeneity, relations and interactions between the mesenchymal and hematopoietic compartments at perinatal stages. To capture the main key features of these processes, we have generated a comprehensive scRNA-seq cellular map of all mouse endochondral bone compartments just before and after birth (E18.5 and postnatal day [PN] 1). The analysis of these datasets, in comparison with those from adult mice (Baccin et al., 2020), uncovers that the composition and molecular fingerprint of several bone populations change significantly between these stages. Of note, our resource study reveals the presence of distinct perinatal fibroblastic mesenchymal populations with molecular signatures that suggest their involvement in the formation of the bone marrow, organization of angiogenesis and peripheral innervation, as well as in the establishment of the environment for proper hematopoiesis, including putative direct interactions between specific mesenchymal and hematopoietic clusters. Notably, our study identifies some mesenchymal clusters with active immunomodulatory transcriptional programs which may be involved in setting an anti-inflammatory setup with implications for the maturation of the immune system and the self from non-self discrimination that is just starting to take shape. Overall, our findings highlight the relevance of integrative ontogenic studies that take into account the full cellular complexity of the endochondral bone and have important implications for the prospective isolation of cell populations for tissue engineering applications as well as for the age-tailoring of disease treatments.

114

115 **RESULTS**

116 **A cell atlas of the perinatal endochondral bone**

117 To get a comprehensive understanding of the composition and dynamics of the
118 endochondral bone in the transition from intrauterine to extrauterine life, with particular
119 emphasis on the mesenchymal compartment, we adopted a FACS-enrichment
120 strategy that ensured that all cellular components of the E18.5 and PN1 endochondral
121 bone (forelimbs excluding the autopod) could be captured by scRNA-seq in a balanced
122 manner. This strategy is similar to that previously employed for adult bone (Baccin et
123 al., 2020), and allows to investigate not only the relationships between mesenchymal
124 subpopulations, but also their involvement in angiogenesis, hematopoiesis, and
125 peripheral nervous system development. To represent both abundant and minor
126 populations, we employed the sorting strategy depicted in Fig. 1A (see also Materials
127 and Methods). Briefly, dead cells and multiplets were excluded by gating, and no
128 lineage labeling was used to prevent the loss of any cell subsets. The gates were
129 defined by the use of a mix of pan-antibodies to mesenchymal (CD140a/PDGFR-a)
130 and endothelial cells (CD31/PECAM), together with CD9, a marker highly expressed
131 in early hematopoietic progenitors and stromal cells (nicheview.shiny.embl.de; Baccin
132 et al., 2020). Sorted cells were mixed in different proportions to better represent less
133 abundant populations (Fig. 1A). While this strategy is not quantitative, it allows
134 monitoring relative changes in cell number between equivalent clusters at both stages.
135 After QC, 7,272 (E18.5) and 7,277 (PN1) high-quality cells were recovered for
136 analysis, with a mean of 2,625 and 2,533 genes per cell, respectively.

137

138 A combination of unsupervised and curated clustering led to the annotation of 24 cell
139 populations, each displaying a distinct molecular signature (Fig. 1B,C, Fig. S1 and Fig.
140 S3). These clusters encompass all hematopoietic, mesenchymal and endothelial
141 compartments in the perinatal endochondral bone. The entire hematopoietic
142 compartment (HC, encircled in dark blue) and each of its clusters are characterized by
143 the expression of defining markers such as *Ptprc* (pan-HC), *Cd79a* (B-Lin), *CD200r3*
144 (Eo-Bas), etc. Recent scRNAseq, scATAC and scProteo-genomic data have

145 demonstrated that FACS-isolated oligopotent progenitors represent heterogeneous
146 mixtures of progenitor populations (Buenrostro et al., 2018; Ranzoni et al., 2021;
147 Triana et al., 2021). Not being our primary focus, we opted for broad categories for the
148 definition of HC clusters. For instance, HPC (hematopoietic progenitor cells)
149 encompasses granulocyte/monocyte progenitors, megakaryocyte progenitors and
150 LMPP (Lymphoid Myeloid Primed Progenitors); likewise the B-Lin cluster includes all
151 stages of B cell maturation. The endothelial compartment consists of a single cluster
152 (EC; encircled in purple in Fig. 1B), defined by the expression of pan-endothelial genes
153 as *Cdh5 or Pecam1*/CD31.
154
155 Within the mesenchymal compartment (MC; encircled in light green), clusters
156 corresponding to fate-committed progenitors or to differentiated cells were readily
157 identified according to their molecular signature (Fig. 1B, C, Fig. S1 and Fig. S3). The
158 chondrogenic (ChC) cluster was defined by the expression of the *Sox9*/*Sox5*/*Sox6* trio,
159 which drives the transcription of *Col2a1, Acan, Col9a1, Col9a2* and *Col9a3* (Akiyama
160 and Lefebvre, 2011). The osteogenic (OsC) cluster was labelled by the expression of
161 *Runx2*, *Osterix*/Sp7, *Bglap*/Osteocalcin, *Spp1*/Osteonectin and *Isbp*/bone sialoprotein
162 (Komori, 2022). Finally, the myofibroblast (Myo) cluster was characterized by the
163 expression of key myogenic genes such as *Pax7*, *Myf5, Msc, Myod1* and *Acta2/aSMA*
164 (Alonso-Martin et al., 2016). In addition, we defined seven closely-associated clusters
165 of fibroblastic nature. These included a cell population with tenogenic characteristics
166 (TC) (Jelinsky et al., 2010; Murchison et al., 2007; Rees et al., 2009; Shukunami et
167 al., 2018; Zhang et al., 2017), expressing *Scx*/Scleraxis, *Tnmd*/Tenomodulin,
168 *Kera/*Keratocan and *Cpxm2*, and an articular cartilage progenitor (ACP) cluster
169 expressing *Sox5*, *Gdf5, Pthlh*, *Barx1*, *Prg4* and *Wnt4* (Fig. 1C, Fig. S1 and Fig. S3)
170 (Chijimatsu and Saito, 2019; Pacifici et al., 2000). We also identified *Tspan15* and
171 *Ackr2* as novel ACP markers, with implications in bone growth and remodeling
172 (Eschenbrenner et al., 2020; Lima et al., 2017; Mizuno et al., 2020). The remaining
173 five mesenchymal clusters were even closer in the UMAP space and annotated as
174 GFP (*Gas6*$^{+}$ Fibroblastic Population, also enriched in *Eln*-expressing cells), SFP (Sca-
175 1*/Ly6a*$^{+}$ Fibroblastic Population, expressing other markers such as *Ly6c1*), AFP
176 (Adipogenic Fibroblastic Population, expressing *Ptch2* and *Notch3*), CLFP (*Cxcl12*-

177 Low Fibroblastic Population, expressing *Ly6h* and *Lpl*) and PFP (Proliferating
178 Fibroblastic Population) (Fig. 1C, Fig. S1 and Fig. S3). The PFP population is
179 composed of cells in S or G2/M phases of the cell cycle and expresses mitogenic
180 genes such as *Mki67, Nusap1, Cenpe* and *Ccna2* (Fig. 1c, Fig. S1 and Fig. S3). PFP
181 contains the proliferating fractions of the GFP, SFP, AFP and CLFP clusters, but
182 minimally of ACP, which fits the long-lasting quiescency of articular progenitors
183 (Decker et al., 2017). Cell-cycle analysis also revealed small proliferating subsets
184 within other hematopoietic and mesenchymal clusters, including ChC and Myo (Fig.
185 S3B and 3C). The comparison of cluster ratios showed changes in both hematopoietic
186 and mesenchymal compartments accompanying the transition to extrauterine life,
187 including a marked increase in the representation of SFP, AFP and TC clusters at PN1
188 when compared to E18.5 (Fig. 1D). Since each sample per stage was obtained by
189 pooling littermate tissue from both sexes, we deconvoluted the scRNA-seq datasets
190 according to the expression of sex-specific genes. All clusters annotated in the pooled
191 samples were identified in both females and males and the trends observed in the
192 SFP, AFP and TC clusters between E18.5 and PN1 were maintained (Fig. S2). Given
193 these results, all downstream analyses were performed using the pooled sample.
194

195 **Highlighting the differences between perinatal and adult bone mesenchymal**
196 **compartments**

197 Next, we used Harmony (Korsunsky et al., 2019; Luecken et al., 2022) to integrate our
198 perinatal scRNA-seq datasets with those previously reported for adult (Baccin et al.,
199 2020), generated from femurs, tibiae, hips and spines from 8-12 weeks old females
200 (Fig. 2, Fig. S4 and Fig. S5). This analysis indicated a good broad correlation between
201 both stages, with related clusters falling into equivalent positions within the integrated
202 UMAP space, with the exception of PFP, which was disconnected from the main
203 fibroblastic clusters and split into three components (asterisks in Fig. 2A). Cell cycle
204 analysis showed that, in contrast to perinatal stages where all compartments are
205 proliferating, only the adult hematopoietic compartment displays cells in S and G2/M
206 phases (Fig. 2B). Focusing on the mesenchymal compartment, adult chondrocytes
207 and myofibroblasts had perinatal counterparts. The closely associated SFP, GFP, AFP
208 and CLFP perinatal clusters localized in similar UMAP coordinates as the adult

endosteal, arteriolar and stromal fibroblasts, while perinatal ACP and TC were not clearly identified in the adult scRNAseq dataset (see Discussion).

One of the most studied bone mesenchymal populations are CARs (*Cxcl12*-abundant reticular cells; Sugiyama et al., 2006). Seminal studies in the last decade have identified their pivotal role in hematopoiesis (Morrison and Scadden, 2014). Adult CARs are also characterized by the expression of *Kitl* and represent almost all LepR+ cells(Fig. 2C) (Ding and Morrison, 2013; Ding et al., 2012). scRNAseq studies have further subdivided CARs in view of their adipogenic (Cxcl12+, Alpl-) or osteogenic profiles (Cxcl12+, Alpl+) (Baccin et al., 2020; Wolock et al., 2019) and even in more subsets (Matsushita et al., 2020; Mo et al., 2022; Tikhonova et al., 2019), reflecting their adipogenic, osteogenic and BMSC differentiation potential. The comparison between equivalent UMAP plot coordinates at perinatal and adult stages (boxed area in Fig. 2C) revealed the almost complete absence of AdipoCARs in the perinatal bone and markers highly detected in adult Adipo-CARs (*Lepr, Cxcl12, Kitl, Pparg, Adipoq and Vcam1/*CD106) (Jeffery et al., 2022; Severe et al., 2019) were expressed in very few cells at perinatal stages, next to the OsC cluster (Fig. 2C). These results suggest that Adipo-CARs are just arising at perinatal stages and are in keeping with other reports using LepR antibodies, *Lepr*-CreER lines induced in the early postnatal life and recent scRNAseq analysis of the stromal compartment at postnatal day four (Kara et al., 2023; Liu et al., 2022; Mizoguchi et al., 2014; Shu et al., 2021). Of note, *Cxcl12, Kitl, Gas6* and *Lpl* were all expressed at lower levels in fibroblastic clusters, mainly in CLFP, AFP and GFP (Fig. 2C and Fig. S4), opening the possibility that some of the Adipo-CAR progenitors could be contained within these clusters. In line with this possibility, also *Pparg* and *LepR*, important players of the adipogenic program that starts to shape perinatally, are expressed in a scattered manner in the perinatal fibroblastic clusters, including AFP cells (Fig. 2C and Fig. S4). In contrast, there is a good correlation between the perinatal OsC cluster and the adult osteogenic cells, which include Osteo-CARs, Ng2+ cells and osteoblasts, with high expression of osteogenic genes (Fig. 2C and Fig. S4). As others have described for adult bone (Baccin et al., 2020; Baryawno et al., 2019; Matthews et al., 2021), we also located the perinatal prospective mSSC (murine Skeletal Stem Cells; Chan et al., 2015),

241 characterized by the immunophenotype CD51+ CD200+; negative for CD45, CD31
242 and TER119, CD90, CD105, 6C3 (Fig. S5A) in the osteogenic-related OsC cluster.
243 The integral analysis of all bone cell populations (Baccin et al., 2020 and this study)
244 also reveals, with high resolution, the spatial and temporal (perinatal versus adult)
245 expression patterns of reported genetic drivers and surface markers, providing an
246 important resource for the interpretation of previous observations using cell-fate
247 tracing mouse models and prospective isolation strategies (Fig. S5). A key advantage
248 of including all bone endochondral populations in scRNA-seq experiments is that it
249 provides a rich resource for the identification of markers restricted to specific
250 populations. To illustrate this point, we identified different genes with preferential
251 expression in the different perinatal fibroblastic clusters, which will allow the design of
252 more precise inducible genetic tools (Fig. S6). Stressing the relevance of performing
253 ontogenic studies, we identified genes active at perinatal stages that are not
254 expressed in the adult tissue.
255
256
257 **The mesenchymal compartment in depth**
258 Next, we generated a new Harmony representation of only the mesenchymal clusters
259 to better illustrate their relations at E18.5 and PN1 (Fig. 3A). As previously mentioned,
260 we observed an increase in SFP and TC populations after birth. In the case of TC
261 (labeled by *Scx* and *Tnmd*), two different branches can be detected. One of these is
262 related to the chondrogenic cluster, while the other branch likely represents tenogenic
263 precursors as is preferentially labelled by additional tendon markers such as *Mkx* and
264 *Kera* (Fig. 3B), and highly-specifically by *Ptx4*, which makes this locus a good
265 candidate for designing genetic tools to study tendon development/regeneration.
266
267 To get insight into the closely connected GFP, SFP, AFP and CLFP clusters, we
268 performed Gene Ontology (GO) analyses starting from their differentially expressed
269 genes E18.5 and PN1 (gene number ranging between 185 and 480; Table S1 and Fig.
270 S7). These results associated CLFP, GFP and SFP to extracellular matrix (ECM)
271 organization and angiogenesis. AFP GO terms link it with the regulation of osteoblast
272 and fat differentiation, as well as with brown fat cell differentiation and cold-induced

273 thermogenesis, the latter term also shared by CLFP and GFP. Fat metabolism is
274 essential in the first hours postpartum, in preparation for starvation and
275 thermoregulation (Hillman et al., 2012; Li et al., 2022b). AFP GO terms also associate
276 it to myeloid and B cell differentiation, branching morphogenesis -a key feature of
277 vessel formation, and glial cell differentiation. SFP GO terms are related to cell
278 migration and cell adhesion, regulation of nitric oxide synthesis, leukocyte
279 differentiation, coagulation and wound healing. GFP displays GO terms for
280 ossification, osteoblast differentiation, response to mechanical stimulus, fibroblast
281 proliferation, cartilage development, hormonal regulation and glucose homeostasis
282 (Morton and Brodsky, 2016). CLFP is also associated to bone mineralization,
283 ossification, glial cell migration (along with SFP), regulation of muscle cell
284 differentiation and axon guidance. This plethora of putative tasks suggests a pivotal
285 role for perinatal fibroblastic clusters in the bone under construction and in the
286 transition to postnatal life. In support for these broad organizing functions, we noted
287 that the perinatal fibroblastic cluster signatures include genes previously identified in
288 the blastema that forms after digit tip amputation in adult mice, including *Mest1*, *Ltbp2*,
289 *Scara5*, *Clec3b* and *Cd34*, the latter three expressed in dermal-derived fibroblasts
290 (Fig. 3C and Fig. S5) (Johnson et al., 2020; Storer et al., 2020).
291
292 **Interactions between endochondral cell subsets and implications for central**
293 **tolerance**
294 To gain insight into the interconnectivity of the different perinatal bone cell populations,
295 we used CellPhoneDB, an algorithm based on the expression pattern of ligands,
296 receptors and ECM components, therefore capturing both direct and indirect
297 interactions (Efremova et al., 2020). The degree of interaction within mesenchymal
298 clusters (MC-MC) and between MC clusters and EC (MC-EC) or hematopoietic
299 clusters (MC-HC) is shown in Fig. 4A. In all three compartments, cluster interactions
300 were higher at E18.5 than at PN1. MC-MC displayed the highest number of calls, being
301 TC, OsC, SFP and GFP the most interacting clusters, and Myo the least. ECM
302 components such as collagens and integrins were the most abundant predicted
303 connectors, as expected for fibroblastic populations, with several stage-specific
304 differences (Tables S2-S4). The type of collagens and integrin complexes was highly

305 diverse and different clusters displayed specific profiles (Table S4), which fits the
306 dynamic properties of the matrisome, which changes according to age and
307 inflammatory conditions (Helbling et al., 2019). For example, a significant difference
308 between E18.5 and PN1 was the lack of integrin a1b1 complex at PN1 in GFP, ACP
309 and OsC clusters. This integrin complex is associated with remodeling and wound
310 healing (Carver et al., 1995). Membrane-bound COL13A1, relevant for bone growth,
311 was mainly expressed by OsC and EC clusters (Kemppainen et al., 2022; Ylonen et
312 al., 2005). This analysis also identified the interconnection of SC with several other
313 subsets through *Col20a1* and a1b1/a2b1 integrin complexes. *Col20a1* is SC-specific
314 and expressed only at perinatal stages (Fig. S1, Fig. S3 and nicheview.shiny.embl.de).
315 As the ECM participates in signaling, migration, lineage specification and
316 compartmentalization in several tissues (Long and Huttner, 2019), these changes
317 might dictate a code involved in the spatial and temporal organization of the skeletal
318 program (Stone et al., 2023).
319
320 Next, we explored direct interactions (no secreted molecules; p-value < 0.05) and
321 focused on those clusters displaying the highest number of partners and the strongest
322 connectors (Fig.4B; all direct connectors are provided in Tables S5 and S6). Within
323 the MC, the SFP and OsC clusters appeared as the most dynamic, with CADM1 and
324 COL13a1 mediating significant interactions in the latter. NOTCH and their ligands
325 were highly expressed among fibroblastic clusters, as expected from their important
326 roles in bone development and homeostasis (Zieba et al., 2020). DLK1-NOTCH1 and
327 DLK1-NOTCH2 mediated very strong connectors in all mesenchymal clusters and with
328 EC (Tables S5 and S6). DLK1 is a non-canonical ligand that inhibits NOTCH1 receptor
329 activity (Gonzalez et al., 2015). Of note, *Dlk1* is not expressed in adult bone
330 (nicheview.shiny.embl.de; Baccin et al., 2020), whereas at perinatal stages it is
331 restricted and highly expressed in most of the clusters of the mesenchymal
332 compartment. NOTCH3 mediated various putative connectors, mainly in AFP, which
333 is relevant as *NOTCH3* mutations cause Lateral Meningocele Syndrome (OMIM
334 #130720), characterized by several skeletal abnormalities (Zieba et al., 2020). In
335 addition, the highly prevalent JAG1-NOTCH3 pair could play a role in vasculature
336 remodeling, as slow-cycling LepR:Cre *Notch3*+ cells were closely associated to

337 vasculature in the bone marrow of adult mice (Mo et al., 2022). In fact, the EC
338 connectome (also explored at E18.5 by Liu et al., 2022), displayed a high number of
339 direct predicted interactions with GFP, OsC, AFP, CLFP and Myo, mainly through
340 selectins (SELL, SELP, SELE), supporting our previous GO analyses that associated
341 AFP and CLFP with different aspects of angiogenesis (Fig. 4B and Fig. S7). Schwann
342 cells (SC) also showed broad potential direct interactions with SFP, AFP, OsC, CLFP
343 and with themselves (Table S5). In particular, we identified a specific link mediated by
344 CADM3 (exclusive of SFP) and CADM4 (exclusive of SC) (Fig. 4C). Future studies will
345 determine the relevance of this interaction, but CADM3 mutations are associated to
346 type 2FF Charcot-Marie-Tooth disease (OMIM #619519), a peripheral neuropathy with
347 early childhood onset and characterized by progressive weakness and muscle atrophy
348 (Rebelo et al., 2021). In this context, both *Col20a1* and *Cadm4* are excellent candidate
349 *loci* for the design of genetic tools to address peripheral nervous system regulation of
350 endochondral bone development and regeneration (Johnston, 2017).
351
352 Concerning the hematopoietic compartment, several of the MC clusters were
353 predicted to interact with HPC, and preferentially with Eo/Bas and ILC-TSP2, being
354 GFP, SFP, AFP and CLFP the most active (Fig. 4A). Representative direct connectors
355 for HPC, ILC-TSP2 and Eo/Bas are APP-CD74, ICAM1-ITGAL and SELL-CD34,
356 respectively (Fig. 4B and Table S6). While adult/perinatal Eo/Bas and B lineage cells
357 map to equivalent coordinates in the UMAP space, there are significant differences
358 between perinatal ILC-TSP2 cells and adult NK and T cells (Fig. 4D and Fig. S8). T
359 cells in the adult bone marrow correspond to memory T cells and regulatory T cells (Di
360 Rosa and Gebhardt, 2016). The T cell cluster in the adult scRNA-seq dataset
361 (nicheview.shiny.embl.de; Baccin et al., 2020) highly expresses all CD3 components
362 of the TCR receptor (*Cd3e*, *Cd3g*, *Cd3d* and *CD247*/TCR zeta) in addition to CD8a
363 and CD8b1, identifying them mostly as memory CD8 T cells. In contrast, perinatal ICL-
364 TSP2 cells only transcribe *Cd3g* and *CD247*, do not express *Lef1* (Shan et al., 2021)
365 and are negative for *Sell*/CD62L and *Ccr7* genes expressed in central memory T cells
366 (Jung et al., 2016). In line with recent scRNAseq data on thymus seeding progenitors
367 (Liu et al., 2021) (TSP), we named this cluster ILC-TSP2 on the basis of the
368 expression of *Cd7, Itgb7, Irf8, CD3e (CD3g* in mouse) and the absence of *Hoxa9* and

369 *Cd34* transcripts (Lavaert et al., 2020; Rothenberg, 2021). Of note, we identified ILC-
370 TSP2 as the only cluster expressing *Ccl5* (Fig. S1 and Fig. S8). This is relevant
371 because callus formation in bone fracture models depend on the expression of the
372 Ccl5 receptors Ccr5 and Ccr3 in periosteal Mx1+Acta2/aSMA+ cells (Ortinau et al.,
373 2019), which highlights the relevance of the crosstalk between the MC and HC (see
374 also additional ILC-TSP2 markers in Fig. S1; Cumano et al., 2019; Zeng et al., 2019).
375 The role of the Eo/Bas cluster at these stages is less characterized. Perinatal Eo/Bas
376 specifically expressed high levels of anti-inflammatory interleukins *Il4* and *Il13* (Fig. S1
377 and Fig. S8). In keeping with an anti-inflammatory setup, we also observed the lack of
378 expression of MHCII genes (*H2-Aa* and *H2-Eb1*) in monocyte and dendritic cells (Mon
379 DC), and a high expression of *Il1rn* and *Il1r2* (both encoding decoy receptors of pro-
380 inflammatory IL1) in monocytes and neutrophil clusters. In addition, monocyte,
381 neutrophil and Eo/Bas clusters express high levels of *Osm* (Oncostatin M), which
382 stimulates osteogenesis and inhibits adipogenesis (Li et al., 2022a), further
383 highlighting the interdependency of the different cellular components (Fig. S8).
384

385 **Main transcriptional networks and immunomodulatory properties of the**
386 **mesenchymal compartment within the perinatal endochondral bone**

387 To shed light on the transcriptional programs operating in the mesenchymal
388 compartment, with special emphasis on the fibroblastic clusters, we utilized SCENIC
389 (Single-Cell rEgulatory Network Inference and Clustering) (Aibar et al., 2017; Van de
390 Sande et al., 2020). This tool can detect the activation of gene regulatory networks
391 controlled by a given transcription factor [called "regulons", noted with a (+) symbol]
392 based on the expression of its cognate targets, even if the upstream TF was not
393 captured in the scRNA-seq data. Conversely, SCENIC labels regulons as not active if
394 not sufficient targets are expressed, even if the controlling TF is detected. The top-ten
395 regulons at E18.5 and PN1 and the differentially active intrauterine and extrauterine
396 regulons are shown in Fig. S9. SCENIC accurately captured biologically relevant
397 regulons in chondrogenic [Sox9(+), Sox5(+); ChC and ACP], osteogenic [Runx2(+),
398 Sp7(+), Dlx5(+); OsC] and adipogenic [Pparg(+), Gata6(+), Prdm6(+); AFP and GFP]
399 clusters (Fig. S10). Concerning the latter differentiation program, *Pparg* is a key
400 adipogenic regulator, while *Gata6* has been recently associated to brown

401 adipogenesis (Rao et al., 2022), in agreement with our GO analysis. Finally, GWAS
402 studies have linked *PRDM6* to obesity and osteoporosis (Hu et al., 2018), and another
403 family member, *Prdm16*, has been implicated in brown fat differentiation in early
404 myoblast progenitors (Seale et al., 2008; Van Nguyen et al., 2020). The CLFP
405 population shared several active regulons with the Myo cluster [MyoG (+), Msc(+),
406 Myf5 (+) and MyoD (+)], suggesting that these two populations could be related.
407 Mkx(+) was the most-significant regulon in TC (Fig. 3) (Liu et al., 2015; Milet and
408 Duprez, 2015). Two additional key observations could be extracted from the SCENIC
409 analysis. Firstly, several Hox regulons were active in GFP, SFP, TC and ACP clusters
410 (Fig. S9). While *Hox* functions have been most studied in the context of axial and limb
411 patterning (Mallo, 2018), it has been described that periosteal Hox+ fibroblastic
412 populations contribute to bone repair in adult fracture models (Rux et al., 2016).
413 Secondly, several of the most prominent regulons in SFP and ACP were related with
414 inflammation and showed multiple cross-regulatory interactions (tables in Fig. 5).
415 *Nfkb1*, one of the most prominent regulons detected by SCENIC, encodes p105 and
416 its processed form p50. Dimers of p65 (the class 2 subunit of NF-κB transcription
417 factor, encoded by *RelA*) and p50 trigger a pro-inflammatory response. The NF-κB
418 pathway is negatively controlled by p50/p50 homodimers that outcompete p65/p50
419 dimers and also suppress pro-inflammatory gene expression by association with other
420 proteins like HDACs and p300 (Cartwright et al., 2016). p50/50 homodimers can also
421 promote the expression of anti-inflammatory genes by association with Bcl3 (Wessells
422 et al., 2004), and the Bcl3(+) regulon itself is active at E18.5 and PN1 and controls
423 *Nfkb1* expression (Fig. 5 and Fig. S9). Another active regulon involved in inflammation
424 regulation and active at E18.5 and PN1 is Atf3(+) (Hai et al., 2010). ATF3 has been
425 shown to inhibit NF-κB pathway by dimerization with p65 and recruiting HDAC1 (Kwon
426 et al., 2015). *Klf3* is a transcriptional repressor that directly suppresses the expression
427 of *RelA* (Knights et al., 2020), and its regulon is active only at E18.5. Of note, the
428 Klf4(+) regulon is detected as active at PN1. In addition to its role in osteogenesis (Abe
429 et al., 2022), *Klf4* participates in several cellular processes depending on the cellular
430 type and context (Ghaleb and Yang, 2017) and it can act as either a pro- or anti-
431 inflammatory factor (Choi et al., 2018; Kawata et al., 2022; Li et al., 2021; Liao et al.,
432 2011). The Cebpd(+) regulon modulates different cellular processes (Balamurugan

433 and Sterneck, 2013), and is mainly related with inflammatory response in
434 macrophages but can also act in preventing deleterious effects of the inflammatory
435 response (Moore et al., 2012; Rustenhoven et al., 2015). Other regulon active only at
436 PN1 and associated with inflammatory regulation is Nr1d1(+) (Nr1d1/Rev-
437 Erbα encodes a core protein of the circadian clock) (Curtis et al., 2014; Liu et al., 2020;
438 Scheiermann et al., 2013). Interestingly, and still not explored in depth, different *Hox*
439 genes interact with the NF-κB pathway and intervene in different aspects of
440 inflammation (Mucientes et al., 2018; Pai and Sukumar, 2020).
441
442
443 **Strategies for the prospective isolation of mesenchymal populations**
444 Based on their molecular profiles, the well-characterized PαS population
445 [immunophenotype: Lineage negative (CD45, TER119, CD31) and PDGFR-a+, Sca-
446 1+] corresponds to the SFP, ACP and part of the GFP clusters. PαS were first
447 described in adult bone (Morikawa et al., 2009) and these Sca-1+ (encoded by *Ly6a*)
448 fibroblastic populations have been shown to contain multipotent progenitors able to
449 give rise to cartilage, bone and adipose tissue (Ambrosi et al., 2017; Ambrosi et al.,
450 2021; Morikawa et al., 2009; Nusspaumer et al., 2017). In addition, Sca1+ cells in the
451 periosteum highly contributed to the formation of the callus in fracture models
452 (Duchamp de Lageneste et al., 2018; Jeffery et al., 2022; Matthews et al., 2021; Mo
453 et al., 2022; Perrin et al., 2023). PαS are most abundant at perinatal stages, peaking
454 immediately after birth and being less represented in adults (Nusspaumer et al., 2017).
455 These properties, together with the immunomodulatory profile of SFP and ACP
456 revealed by the SCENIC analysis, make PαS an important target for biomedical
457 applications. Hence, developing robust isolation strategies is key for the isolation of
458 the human equivalent populations for use in cellular therapies, but as there is no
459 human ortholog of the *Ly6a*/Sca-1 gene (Lee et al., 2013), additional reliable markers
460 need to be identified. To do so, we interrogated our scRNA-seq datasets for several
461 surface markers that were evolutionary conserved between mouse and human and
462 validated them by FC in order to develop an alternative isolation strategy to enrich in
463 PαS cells without resorting to the use of Sca-1 antibodies. The final strategy and best
464 markers assayed to enrich in SFP, ACP and CLFP populations from newborn bone

465 are shown in Fig. 6. All lineage negative *Ly6a*/Sca-1+ cells were PDGFR-α+ (Pa+),
466 *Pdpn*/gp38+, *Cd55*+ and mostly *Entpd1*/CD39 negative (Fig. 6A). CD39+ Pa+ defined
467 the CLFP population, while CD55 was highly expressed in ACP and SFP, with
468 *Thy1*/CD90 only labeling SFP (Fig. 6A and 6B). These profiles allowed devising a
469 strategy to purify CLFP, SFP and ACP populations in three steps (Fig. 6C). The
470 separation between SFP (CD90+) and ACP ($CD90^{neg}$) within $CD55^{hi}$ cells was
471 confirmed using Sca-1 and CD90 staining. While this strategy is suitable for perinatal
472 stages, *Entpd1*/CD39 is hardly expressed in mesenchymal adult populations (Fig. 6A),
473 which illustrates the importance of performing ontogenic studies and adapt the
474 prospective immunophenotype to the specific stage under analysis.
475

476 **DISCUSSION**

477 As previous scRNAseq studies have shown, the adult bone mesenchymal
478 compartment is very diverse and this resource study uncovers how such complexity
479 starts to build up in early life. Our analysis reveals different clusters of fibroblastic
480 populations at perinatal stages, with diverse potentials as indicated by GO and gene
481 regulatory network tools. These analyses unveiled that the most closely related
482 fibroblastic clusters (GFP, SFP, AFP and CLFP), in addition to their potential to
483 regulate osteogenesis, adipogenesis and chondrogenesis, may also be involved in a
484 wide spectrum of tissue-organizing functions, including the regulation of
485 hematopoiesis, angiogenesis, innervation, extracellular matrix organization,
486 metabolism and hemostasis. For instance, AFP representation increased after birth
487 and, along with the GFP population, is associated to adipogenesis, including brown
488 fat differentiation and cold-induced thermogenesis, so important to control caloric
489 restriction and temperature once the protection of the placenta is lost (Hillman et al.,
490 2012). LepR+ CAR cells, highly represented in adults (Gomariz et al., 2018), were not
491 present at perinatal stages. This is not due to the enrichment strategy used, since this
492 population was barely detected by FC from total bone enzymatic cell suspensions
493 using the CD106/Vcam1 Adipo-CARs marker (data not shown). Our findings are in
494 line other studies (Kara et al., 2023; Liu et al., 2022), which show that Adipo-CARs
495 are absent a E18.5 and just emerging at postnatal day 4. Interestingly, AFP could

496 represent a precursor of Adipo-CARs, since it was the main and almost exclusive
497 cluster expressing *Notch3*. *Notch3*-expressing cells targeted by LepRCre in adults
498 showed to be multipotential slow cycling cells (Mo et al., 2022). Two other clusters that
499 were more prominent after birth were SFP and TC. While the absence of an equivalent
500 TC cluster in adults could be related to differences in sample preparation methods or
501 in the origin of bones used, both TC and several of the fibroblastic clusters displayed
502 differential molecular fingerprints previously identified as specific of the blastema
503 during digit tip regeneration in adult mice (e.g. *Mest* expression). These results fit the
504 previous observation that digit tip blastema cells are more similar to bone-derived
505 mesenchymal cells at PN3 than to those of adult and largely differ from those of the
506 limb bud (Storer et al., 2020). In amphibian limb amputation models, successful
507 regeneration requires the dedifferentiation of connective tissue and dermal fibroblasts
508 in order to rebuild the skeleton (Lin et al., 2021). Hence, the complex set of perinatal
509 fibroblastic populations we have identified in this study -some of which also have
510 dermal signatures- may act as reprogramming, specification and differentiation
511 organizers of bone structure during these dynamic stages in which the bone marrow
512 is under active construction to establish definitive hematopoiesis and during which
513 osteo-chondrogenic programs are very active. The granularity of our study allowed the
514 identification of various fibroblastic populations with distinct molecular identities and
515 putative roles in these organizative processes, and our profiling of markers and active
516 gene regulatory networks provides an entry point for the prospective isolation -as we
517 show for SFP, ACP and CLFP- and *in vitro* expansion of some of these specific cell
518 subsets for tissue engineering approaches. Besides, the identification of cluster-
519 specific genes will allow the design of more precise inducible genetic mouse lines for
520 cell fate tracking or cell population depletion. As the system reaches the steady state
521 after sexual maturity, these fibroblastic populations become less abundant in the inner
522 bone marrow, being associated to the endosteum and periosteum and obtained mainly
523 by enzymatic digestion of the bone chips (Duchamp de Lageneste et al., 2018;
524 Guarnerio et al., 2014). Concomitantly, BMSC (such as LepR+ CARs) become
525 prominent (Jeffery et al., 2022; Mizoguchi et al., 2014; Mo et al., 2022; Omatsu et al.,
526 2010; Shu et al., 2021). Only if the balance is broken, as demonstrated by bone
527 fracture models, periosteal cells (e.g. with the PαS immunophenotype) and probably

528 nearby connective tissue cells (Lin et al., 2021) reactivate the endochondral bone
529 program for callus formation (Duchamp de Lageneste et al., 2018; Jeffery et al., 2022;
530 Matsushita et al., 2021; Matthews et al., 2021; Perrin et al., 2023; Zhou et al., 2014).
531
532 Our integral approach to capture all endochondral bone cell populations also allowed
533 us to predict intra- and inter-compartment interactions of all mesenchymal clusters.
534 For instance, in this study we identified that *Cadm3*, the ortholog of the human gene
535 mutated in Charcot-Marie-Tooth type 2FF peripheral neuropathy (Rebelo et al., 2021),
536 is specifically expressed by the SFP population and mediates a putative direct
537 interaction with Schwann cells via CADM4. These analyses also unveiled a potentially
538 complex MC-HC connectome, inferring interactions of fibroblastic SFP, AFP, CLFP
539 and GFP populations with HPC and, more unexpectedly, with the ILC-TSP2 and
540 Eo/Bas clusters. From the immune perspective, these ILC-TSP2 interactions might
541 play a role in the protection/maturation of thymus seeding progenitors for the
542 establishment of central tolerance in the thymus and the generation of the first thymic
543 regulatory T cells (Sakaguchi et al., 1982; Yang et al., 2015). This hypothesis is
544 supported by the recent identification of two populations of mesenchymal cells
545 essential for thymus development with prospective signatures similar to those of bone
546 GFP and SFP clusters (Ferreirinha et al., 2022). Concerning the Eo/Bas cluster, we
547 observed a high and exclusive expression of anti-inflammatory cytokines *Il4* and *Il13*.
548 In line with our observations, basophil cells in newborns were shown to skew the
549 differentiation of T cells towards Th2, which in newborns have an anti-inflammatory
550 profile to protect intestinal microbiota and prevent tissue damage (Dhakal et al., 2015;
551 Luo et al., 2023). Highlighting the predicted interdependency between compartments,
552 both hematopoietic clusters also express key factors mediating bone healing (*Ccl5*
553 (Ortinau et al., 2019) in ILC-TSP2) and osteogenesis-adipogenesis balance (*Osm* (Li
554 et al., 2022a) in Eo/Bas). Future studies will be required to address the potential
555 relevance of these bi-directional interactions at perinatal, puberty and adult stages.
556
557 Another important finding from our study is the identification of several
558 immunomodulatory transcriptional programs operating in mesenchymal clusters (SFP,
559 ACP and, to some extent, GFP) that seem to be skewed towards an anti-inflammatory

560 response. These observations fit the previous proposal that the 2-week juvenile mouse
561 bone provides an anti-inflammatory environment (with low expression of MHCI
562 molecules in stromal populations) that changes to pro-inflammatory after sexual
563 maturation (Helbling et al., 2019). In support of this, several mesenchymal clusters
564 highly express *Dlk1*, a ligand previously shown to inhibit Notch-dependent pro-
565 inflammatory cytokine production by macrophages (Gonzalez et al., 2015). In contrast
566 to adult populations, perinatal macrophages neither express MHCII genes (*H2E-b1*
567 and *H2A-a*) nor their protein products (also assessed by FC; data not shown), while
568 neutrophils display high expression of the IL-1 decoy receptors *Il1rn* and *Il1r2.* An
569 attractive hypothesis stemming from our results is that an anti-inflammatory
570 environment of the perinatal bone marrow could ensure the proper balance between
571 myeloid and lymphoid HSC lineage choice. High pro-inflammatory conditions promote
572 HSC division and skew their differentiation towards the myeloid lineage at the expense
573 of lymphopoiesis, potentially leading to excessive proliferation and exhaustion of HSC
574 (Ho and Takizawa, 2022). In addition, and particularly in early life where individuals
575 are first exposed to pathogens, primary immune organs (bone marrow and thymus)
576 should be protected from infections and the deleterious effects of a highly pro-
577 inflammatory milieu, to ensure the establishment of a proper self-tolerance.
578
579 Finally, our study reveals significant cellular and gene expression differences between
580 neonatal and adult stages which implies that therapeutical interventions targeting
581 endochondral bone populations or compartments must be adapted according to the
582 age of the patient. While our work is limited by the lack of functional validation of the
583 main findings and the fine spatial localization of each specific cluster we identify, it
584 provides a valuable resource that highlights key aspects of endochondral bone
585 development for the broader research community to further investigate in depth.
586
587
588
589
590
591

592

593 **MATERIALS AND METHODS**

594

595 **Mice (*Mus musculus*)**

596 Adult C57Bl/6J females and males were purchased from Envigo and housed under
597 pathogen-free conditions according to Spanish and EU regulations. All animal
598 experiments were designed according to the 3R principles and approved by the local
599 Ethics Committee and authorities (license 01-08-2018-123). Animals were set in
600 natural matings and vaginal plugs checked to time the collection of samples at E18.5
601 and postnatal day 1 (considering the day of birth as postnatal day 0). Individuals of
602 both sexes were used for scRNA-seq experiments and flow cytometry studies.

603

604 **Tissue processing for flow cytometry**

605 Forelimb long bones (humerus, radius and ulna) were dissected from fetuses at
606 embryonic day E18.5 and pups at postnatal day 1 and carefully cleaned of surrounding
607 tissue. Cell suspensions for flow cytometry (FC) analysis or sorting were prepared as
608 previously reported (Houlihan et al., 2012), with the following specific modifications.
609 For perinatal stages, bones were cut in small pieces with a scalpel and all tissue was
610 processed (bone marrow cells were not washed out or flushed) for enzymatic digestion
611 using collagenase D (2mg/ml in DMEM [high glucose]). Red cell lysis was not
612 performed. The time of digestion for perinatal stages was 45-50 minutes in a water
613 bath at 37ºC with 3 rounds of gentle pipetting every 10 min to help disaggregation.
614 Collagenase digestion was stopped in ice and by addition of ice-cold 10%FBS/HBSS+
615 (HBSS, 10mM HEPES, 1% Penicillin-Streptomycin). Cells in suspension were
616 recovered to a new tube and any remaining bone pieces were transferred to a ceramic
617 mortar and 2 to 3 steps of very gentle tapping with the pestle (20-30 times) was applied
618 to increase cell recovery. Cells in the mortar were recovered with the addition of
619 10%FBS/HBSS+, filtered through a 100μm strainer and pooled with the cell
620 suspension set aside. After centrifugation (350g for 10 min at 4°C), cells were
621 resuspended in 2%FBS/HBSS+ for FC analysis or sorting. Before antibody staining,
622 blocking of FcγR II/III was performed by incubation in ice with anti-CD16/CD32
623 antibodies for 15 min (1mg/million cells). Collection tubes for sorting were precoated

624 for 15 minutes with 10% FBS/HBSS+ in ice, and kept at 4º C during sorting. Samples
625 were analyzed and sorted in a SONY MA900 (lasers: 488/561 and 405/638nm). 7-
626 AAD (7-amino actinomycin D) was the only dye used to discriminate dead cells. The
627 lineage cocktail to analyze mesenchymal populations included CD45 (hematopoietic
628 cells), TER119 (erythroid cells) and CD31 (endothelial cells), all conjugated to biotin
629 and detected via secondary staining with Streptavidin-PECy7. Lowly-expressed
630 molecules were stained with antibodies conjugated either with BV421 (not used when
631 PB was selected), PE or APC, while highly expressed molecules were stained with
632 antibodies conjugated either with PB (not used when BV421 was selected), FITC,
633 BV785 or A700 fluorophores. All antibodies used are referenced in Table 1.
634

Table 1. Antibodies used in this study	**Biolegend Cat. No.**
FITC anti-mouse CD9 (clone MZ3)	124807
Brilliant Violet 421™ anti-mouse CD140a (clone APA5)	135923
APC anti-mouse CD140a (clone APA5)	135907
APC anti-mouse CD31 (clone 390)	102409
Brilliant Violet 785™ anti-mouse Ly-6A/E (Sca-1) (clone D7)	108139
Alexa Fluor 700 anti-mouse CD90.2 (Thy-1.2) (clone 53-2.1)	140323
FITC anti-mouse Podoplanin (clone 8.1.1)	127415
APC anti-mouse CD39 (clone Duha59)	143809
PE anti-mouse CD55 (DAF) (clone RIKO-3)	131803
Biotin anti-mouse TER-119/Erythroid Cells (clone TER-119)	116204
Biotin anti-mouse CD31 (clone 390)	102404
Biotin anti-mouse CD45 (clone 30-F11)	103104

635
636
637 **Flow cytometry analysis**
638 Data was acquired with a SONY MA900 using the equipment's software and further
639 analyzed using FlowJo v10.8.0. Representative plots of at least three independent
640 experiments are shown.
641

642 **Generation of single cell RNA-seq datasets**

643 Five embryos E18.5 and four newborns PN1, all littermates, were processed for cell
644 suspension preparation as described above. No sex discrimination was done since at
645 perinatal stages gender associated differences are not highly relevant. After
646 eliminating dead cells and multiplets by electronical gating, the different fractions of
647 sorted cells (100μm nozzle) were mixed in the proportions detailed in Fig. 1A. Cells
648 were sorted in excess (~5X more than calculated) to account for cell loss. Absence of
649 cell aggregates was confirmed by microscopic visualization, and cell number and
650 viability were assessed in a TC-20 cell counter (Bio-Rad) with trypan blue staining. For
651 both E18.5 and PN1 samples, viability was > 90%. Cells were resuspended in HBSS+
652 2%FBS at 800 cells/μl and 20.000 cells were loaded in a Chromium Controller G chip
653 (10x Genomics) and processed with the Chromium Next GEM Single Cell 3' Kit v3.1
654 for the generation of the scRNAseq libraries in parallel, according to the
655 manufacturer's protocol. Libraries were sequenced on a DNBSEQ-T7 system
656 (PE100/100/10/10; sequencing performed by BGI). Depth of sequencing was 43,005
657 and 43,398 reads/cell at E18.5 and PN1, respectively (60% saturation). It should be
658 noted that this kit captures the 3'UTR of transcripts, and therefore cannot detect
659 alternative mRNA isoforms.

660

661 **Analysis of single cell RNA-seq datasets**

662 Pre-processing of scRNAseq data. Reads were aligned to the mouse genome (mm10)
663 with the Cell Ranger v6.0 software. Cells with fewer than 400 or more than 6,000
664 detected genes, or more than 10% of mitochondrial reads were excluded. For
665 normalization, log-transformation with a scale factor of 10,000 was used.

666 Dimensional reduction and clustering. 2,000 top high variable genes (HVG) were
667 identified with the "vst" method of the *FindVariableFeatures* function of the Seurat
668 package (version 4.0.3; Hao et al., 2021). The data were scaled and PCA (30 PCs)
669 performed. The cells were clustered using the Louvain Method on a nearest neighbor
670 graph using the *FindClusters* and *FindNeighbors* in Seurat. A UMAP on the PCA
671 reduced data was performed to visualize the clusters.

672 Elimination of erythroid cells and doublets. Based on gene markers, erythroid cells
673 were removed from downstream analyses. For doublet removal, the software

674 DoubletFinder (McGinnis et al., 2019) was used. After filtering low-quality cells,
675 putative doublets and erythroid cells, our dataset contained 7,272 cells with 10,656
676 mean number of reads and 2,625 mean number of genes for E18.5 and 7,277 cells
677 with 9,827 mean number of reads and 2,533 mean number of genes in PN1. As both
678 datasets were generated by pooling littermates of both sexes, we used sex-specific
679 transcripts (*Xist, Esr1* and *Esr2* [female]; *Ddx3y, Eif2s3y, Kdm5d* and *Uty* [male]; Shay
680 et al., 2020) to identify if any given cell was derived from a female or a male individual.
681 More specifically, we assigned a "female" or "male" sex to a cell if it had at least one
682 transcript read from a female or male specific transcript, respectively. If cells had at
683 least one transcript read from both male and female specific transcripts the cell was
684 tagged as "undetermined". Cells without any sex-specific transcript reads were tagged
685 as "NA". For the E18.5 sample we identified 21% female cells, 42% male cells, 3.7%
686 undetermined and 33.3% NA cells. For the PN1 sample we identified 42.3% female
687 cells, 28.1% male cells, 4.4% undetermined and 25.2% NA cells.
688 Sample integration. In order to jointly analyze both E18.5 and PN1 samples, data were
689 integrated with the Harmony software (Korsunsky et al., 2019) and projected into a
690 shared 2D UMAP embedding. Briefly, the Harmony algorithm can integrate samples
691 accounting for multiple experimental and biological factors using an iterative approach
692 of four steps. 1) PCA for a low-dimensional embedding of cells from the different
693 samples and soft clustering to assign cells to potentially multiple clusters favoring
694 clusters with cells from multiple samples. 2) Global and sample-specific centroids are
695 calculated for each cluster. 3) Centroids are used to compute linear correction factors.
696 4) Finally, it corrects each cell with a cell-specific factor that is a linear combination of
697 sample correction factors weighted by the soft cluster assignment of the cell. For the
698 comparison of perinatal with adult, we used Harmony to integrate both perinatal
699 samples with the adult dataset (Baccin et al., 2020). The adult data is available to
700 download as a Seurat object from https://nicheview.shiny.embl.de.
701 Cell type annotation. Marker genes described in the extensive literature were used for
702 cluster identification. Although most of the cell types were annotated using a given
703 clustering resolution, subsequent refinement was done through sub-clustering
704 (*FindSubCluster* function of Seurat) and re-annotation.

705 Inference of cell-cell interactions. CellPhoneDB v.2 (Efremova et al., 2020) was used
706 to infer cell-cell connections. To prepare the data for the CellPhoneDB analysis,
707 mouse gene IDs were converted to their human orthologs and count data exported as
708 h5ad format. CellPhoneDB statistical analysis was used to evaluate for significant
709 interactions between predefined cell type pairs. For the quantification of the total
710 number of interactions, we selected a p-value ≤0.05. For direct interactions (Table S5
711 and S6), we considered only connectors with no secreted molecules and p-value ≤0.05
712 and Log2 mean > -1.
713 Gene Regulatory Network analysis. Mesenchymal clusters were extracted and
714 reprocessed as before (i.e. HVG, PCA, clustering, UMAP) and inference of gene
715 regulatory networks and regulon analysis was performed using the pySCENIC
716 software v.0.11.2 (Van de Sande et al., 2020) using default settings.
717
718 **Gene ontology analysis**
719 Differentially expressed genes (DEG) for each of the mesenchymal GFP, SFP, AFP
720 and CLFP clusters at E18.5 and PN1 were obtained using the FindAllMarkers()
721 function in Seurat, using the default parameters (by default Seurat uses the Wilcoxon
722 Rank Sum test for statistical testing). The test was run separately for each timepoint
723 and the resulting DEG were filtered to include only genes with an adjusted p-value
724 <0.005. The resulting number of genes used for GO analysis at E18.5/PN1 (Table S1)
725 was 218/280 (AFP), 455/480 (CLFP), 185/234 (GFP) and 436/305 (SFP). GO terms
726 for the "Biological Process" category were retrieved from http://geneontology.org,
727 filtered by a ratio Fold Enriched/Expected ≥ 2 and manually curated. Plots were
728 generated using the ggplot2 tool for R, representing the -log10 (p values < 0.05), and
729 the overlap was calculated using the number of genes identified in the GO term for
730 each cluster.
731
732
733
734

ACKNOWLEDGMENTS

We thank the rest of the members of the groups for scientific discussions and technical help. We are also grateful to A. Franco, C. Mateos, A. López, P. López and L. Pérez for excellent mouse husbrandy as well as the rest of the CABD Core services, in particular C. Díaz (Flow Cytometry Facility).

COMPETING INTERESTS

No competing interests declared

AUTHOR CONTRIBUTIONS

Conceptualization, G.N and J.L-R; Software, I.S.M and I.C; Formal Analysis, G.N, I.S.M, A.D.R, and J.J.T.; Investigation, G.N, A.D.R., I.S-A, A.A.C, A.F-M, A. M, A.M.B. and J.L-R; Writing – Original Draft, G.N, and J.L-R.; Writing – Review & Editing, all authors; Supervision, H.H, J.J.T, J.L-R., and G.N.; Funding Acquisition, H.H, J.J.T, J.L-R., and G.N.

FUNDING

This work was supported by the Junta de Andalucía (PY20-00421 to J.L-R) and the Spanish Ministerio de Ciencia e Innovación (María de Maeztu Institutional Grant CEX2020-001088-M to J.L-R and J.J.T).

DATA AND CODE AVAILABILITY

- Single-cell RNA-seq data have been deposited in the GEO database (accession number GSE232202) and are publicly available as of the date of publication. Flow cytometry data reported in this paper will be shared by the corresponding authors upon request.
- All scripts necessary to replicate our analysis are available in the following Github repository (https://github.com/irepansalvador/stromal_cells.git) and is publicly available as of the date of publication.

762 **FIGURE LEGENDS**

763 **Fig. 1. A cell atlas of the perinatal endochondral bone**

764 (A) Gating strategy for the processing of cell suspensions for scRNA-seq, obtained
765 after enzymatic digestion of forelimb long bones at E18.5 and PN1 (see Materials and
766 Methods for details). The number of sorted cells that were mixed for each gate is
767 indicated by the color codes in the FC pseudocolor plots. (B) Uniform Manifold
768 Approximation and Projection (UMAP) of annotated clusters at E18.5 and PN1 after
769 Harmony integration. Mesenchymal cells (MC) are encircled in green, hematopoietic
770 cells (HC) in dark blue, endothelial cells (EC) in magenta and Schwann cells (SC) in
771 turquoise. Neu: neutrophils; Ery: erythrocytes; Im Neu: immature neutrophils; HPC:
772 hematopoietic progenitor cells; PHP: proliferating hematopoietic progenitors;
773 ILC_TSP2: innate lymphoid cells and thymic seeding progenitors 2; Eo Bas:
774 eosinophils and basophils; Sca1 HC: Sca-1^{+} hematopoietic cells; Mon DC: monocytes
775 and dendritic cells; Oc: osteoclasts; B Lin: B-cell lineage; SC: Schwann cells; PFP:
776 proliferating fibroblastic population; ACP: articular cartilage population; TC: tenogenic
777 cells; SFP: Sca-1^{+} fibroblastic population; GFP: *Gas6*$^{+}$ fibroblastic population; AFP:
778 adipose fibroblastic population; CLFP: *Cxcl12*-low fibroblastic population; ChC:
779 chondrogenic cells; OsC: osteogenic cells; Myo: myofibroblasts. (C) Dotplot of the
780 representative genes across perinatal (E18.5 and PN1) clusters. Dot color and size
781 indicate average expression levels and percentage of cells in a cluster expressing the
782 selected gene, respectively. Gene expression is normalized and scaled to that of the
783 entire dataset (mean=0; s.d=1), so negative values correspond to expression levels
784 that are lower than the mean expression in the dataset. (D) Stacked-bar charts
785 indicating the proportions of cells assigned to each cluster at E18.5 and PN1.

786

787 **Fig. 2. Differences between perinatal and adult bone.**

788 (A) UMAP plot of Harmony-integrated adult (Baccin et al., 2020) and perinatal
789 scRNAseq datasets. Note that the integration with adult data changes the distribution
790 of the clusters in comparison to Fig. 1 (e.g. PFP, indicated by asterisks). PChC:
791 proliferating chondrogenic cells. (B) Cell cycle analysis of the Harmony-integrated
792 adult and perinatal scRNAseq datasets. Arrowheads and dotted lines indicate G2/M
793 clusters that in adult correspond to HC (*Ptprc*+ and *Spn*+) and that in perinatal stages

794 is part of the PFP mesenchymal cluster (positive for *Pdgfra+* and *Prrx1+*). (C) Genes
795 expressed in adult CARs and its expression at perinatal stages (upper panels). Lower
796 left box: enlarged view to compare the coordinates of AdipoCARs in adult and their
797 absence in perinatal stages. Lower right panel: magnification of CAR clusters and
798 overlay of adult Adipo- and OsteoCARs markers with the perinatal bone cellular map.
799
800 **Fig. 3. Hierarchy between mesenchymal clusters of the perinatal bone**
801 (A) Harmony integration of mesenchymal clusters at E18.5 and PN1. The two
802 branches of the TC cluster at PN1 are labeled by a dotted line. (B) Expression of TC-
803 specific genes at E18.5 and PN1. Enclosed in a red dotted line is *Ptx4*, a gene
804 exclusively expressed in the tenogenic branch. (C) Expression in perinatal and adult
805 bone of genes identified in dermal and blastema cells in the mouse digit tip
806 regeneration model.
807
808 **Fig. 4. Cell to cell communication in the perinatal endochondral bone**
809 (A) Heatmap showing the total number of connections (Nº of calls; p-val≤0.05)
810 identified by the CellPhoneDB algorithm within mesenchymal clusters (MC-MC),
811 between mesenchymal clusters and EC (MC-EC) and mesenchymal and
812 hematopoietic clusters (MC-HC). (B) Bubble plot representation of selected putative
813 direct interactions (rows) inferred with CellPhoneDB (no secreted molecules; p-value
814 ≤0.05) at E18.5 showing the mesenchymal clusters (clusters) with the higher number
815 of associations within the mesenchymal compartment (MC-MC), with endothelial cells
816 (MC-EC) and with hematopoietic clusters (MC-HC). Dot size represents the mean
817 fraction of cells in the group (cluster1 and cluster 2) expressing molecule 1 and
818 molecule 2. Color encodes the scaled mean expression levels of interacting molecules
819 in the group. (C) UMAP projection at E18.5 showing the exclusive expression of
820 *Cadm3* and *Cadm4* in SFP and SC, respectively, identified by CellPhoneDB as a
821 putative direct interaction between these clusters. (D) UMAP coordinates comparing
822 Eo/Bas, NK-Tcells versus ILC-TSP2 and B-cell clusters in perinatal and adult bone.
823 Striking differences are observed between NK-T cells versus ILC-TSP2 (enclosed in
824 red dotted box and indicated by red arrows).
825

826 **Fig. 5. Immunomodulatory properties of the perinatal bone mesenchymal**
827 **compartment**
828 (A, B) SCENIC analysis of the MC at E18.5 (A) and PN1 (B) displaying the main
829 immunomodulatory regulons. UMAP projections of the mesenchymal clusters at E18.5
830 and PN1 are shown as a guide for cluster identification. The tables show the regulons
831 that control the expression of key transcription factors involved in immunomodulation
832 (*Klf3*, *Klf4*, *Nfkb1*, *Cebpd* and *Nr1d1*). Colored in red are their regulons to show their
833 autoregulation and the network of cross regulation. Lower panels depict the joint
834 activity of the regulons Atf3(+), Nfkb1(+) and Klf3(+) at E18.5 and Atf3(+), Nfkb1(+)
835 and Klf4(+) at PN1. The individual expression of the corresponding genes is displayed
836 to the right of each SCENIC projection.
837
838
839 **Fig. 6. Prospective identification of ACP, SFP and CLFP clusters in newborns**
840 (A) Expression of surface markers suitable for FC analysis at perinatal stages. PαS
841 (PDGFRa+, Sca-1+) cells encompasses clusters SFP and ACP. In addition,
842 *Ly6a*/Sca1 is expressed in EC and Sca1HC. *Cd55* mirrors well the expression of *Ly6a*
843 in the mesenchymal clusters. Within mesenchymal clusters, *Entpd*/Cd39 mainly
844 identifies CLFP, while *Thy1/*CD90 is restricted to SFP. The expression of these same
845 genes in adult bone is shown in the bottom row. (B) FC analysis comparing the
846 expression of Sca-1 with the other prospective markers (CD55, CD39 and CD90) in
847 the mesenchymal compartment (Lin^{neg} PDGFR-a+/Pa+ and gp38/Pdpn+). Dead cells
848 were excluded as 7-AAD positive. Lin= Lineage (TER119, CD45 and CD31). (C) A 3-
849 step strategy not relying on the use of Sca-1 to enrich in SFP, ACP and CLFP
850 populations. SFP (Lin^{neg} $PDGFRa^{+}$ $gp38^{+}$ $CD39^{neg}$ $CD55^{+}$ $CD90^{+}$); ACP (Lin^{neg}
851 $PDGFRa^{+}$ $gp38^{+}$ $CD39^{neg}$ $CD55^{+}$ $CD90^{neg}$); CLFP (Lin^{neg} $PDGFRa^{+}$ $gp38^{+}$ $CD39^{pos}$).
852 Pseudocolor plots are representative of at least 3 independent experiments at PN1,
853 each cell sample extracted from to 3-4 littermates. Similar results were obtained with
854 E18.5 samples (data not shown).
855
856
857
858

859 **REFERENCES**

860

861 **Abe, M., Saeki, N., Ikeda, Y. and Ohba, S.** (2022). Kruppel-like Factors in Skeletal
862 Physiology and Pathologies. *Int J Mol Sci* **23**.

863 **Aibar, S., Gonzalez-Blas, C. B., Moerman, T., Huynh-Thu, V. A., Imrichova, H.,**
864 **Hulselmans, G., Rambow, F., Marine, J. C., Geurts, P., Aerts, J., et al.**
865 (2017). SCENIC: single-cell regulatory network inference and clustering. *Nat*
866 *Methods* **14**, 1083-1086.

867 **Akiyama, H. and Lefebvre, V.** (2011). Unraveling the transcriptional regulatory
868 machinery in chondrogenesis. *J Bone Miner Metab* **29**, 390-395.

869 **Alonso-Martin, S., Rochat, A., Mademtzoglou, D., Morais, J., de Reynies, A.,**
870 **Aurade, F., Chang, T. H., Zammit, P. S. and Relaix, F.** (2016). Gene
871 Expression Profiling of Muscle Stem Cells Identifies Novel Regulators of
872 Postnatal Myogenesis. *Front Cell Dev Biol* **4**, 58.

873 **Ambrosi, T. H., Scialdone, A., Graja, A., Gohlke, S., Jank, A. M., Bocian, C.,**
874 **Woelk, L., Fan, H., Logan, D. W., Schurmann, A., et al.** (2017). Adipocyte
875 Accumulation in the Bone Marrow during Obesity and Aging Impairs Stem Cell-
876 Based Hematopoietic and Bone Regeneration. *Cell Stem Cell* **20**, 771-784
877 e776.

878 **Ambrosi, T. H., Sinha, R., Steininger, H. M., Hoover, M. Y., Murphy, M. P., Koepke,**
879 **L. S., Wang, Y., Lu, W. J., Morri, M., Neff, N. F., et al.** (2021). Distinct skeletal
880 stem cell types orchestrate long bone skeletogenesis. *Elife* **10**.

881 **Baccin, C., Al-Sabah, J., Velten, L., Helbling, P. M., Grunschlager, F., Hernandez-**
882 **Malmierca, P., Nombela-Arrieta, C., Steinmetz, L. M., Trumpp, A. and Haas,**
883 **S.** (2020). Combined single-cell and spatial transcriptomics reveal the
884 molecular, cellular and spatial bone marrow niche organization. *Nat Cell Biol*
885 **22**, 38-48.

886 **Balamurugan, K. and Sterneck, E.** (2013). The many faces of C/EBPdelta and their
887 relevance for inflammation and cancer. *Int J Biol Sci* **9**, 917-933.

888 **Baryawno, N., Przybylski, D., Kowalczyk, M. S., Kfoury, Y., Severe, N.,**
889 **Gustafsson, K., Kokkaliaris, K. D., Mercier, F., Tabaka, M., Hofree, M., et**
890 **al.** (2019). A Cellular Taxonomy of the Bone Marrow Stroma in Homeostasis
891 and Leukemia. *Cell* **177**, 1915-1932 e1916.

892 **Bianco, P. and Robey, P. G.** (2015). Skeletal stem cells. *Development* **142**, 1023-
893 1027.
894 **Buenrostro, J. D., Corces, M. R., Lareau, C. A., Wu, B., Schep, A. N., Aryee, M. J.,**
895 **Majeti, R., Chang, H. Y. and Greenleaf, W. J.** (2018). Integrated Single-Cell
896 Analysis Maps the Continuous Regulatory Landscape of Human Hematopoietic
897 Differentiation. *Cell* **173**, 1535-1548 e1516.
898 **Cartwright, T., Perkins, N. D. and C, L. W.** (2016). NFKB1: a suppressor of
899 inflammation, ageing and cancer. *FEBS J* **283**, 1812-1822.
900 **Carver, W., Molano, I., Reaves, T. A., Borg, T. K. and Terracio, L.** (1995). Role of
901 the alpha 1 beta 1 integrin complex in collagen gel contraction in vitro by
902 fibroblasts. *J Cell Physiol* **165**, 425-437.
903 **Chan, C. K., Seo, E. Y., Chen, J. Y., Lo, D., McArdle, A., Sinha, R., Tevlin, R., Seita,**
904 **J., Vincent-Tompkins, J., Wearda, T., et al.** (2015). Identification and
905 specification of the mouse skeletal stem cell. *Cell* **160**, 285-298.
906 **Chijimatsu, R. and Saito, T.** (2019). Mechanisms of synovial joint and articular
907 cartilage development. *Cell Mol Life Sci* **76**, 3939-3952.
908 **Choi, S., Lee, K., Jung, H., Park, N., Kang, J., Nam, K. H., Kim, E. K., Ju, J. H. and**
909 **Kang, K. Y.** (2018). Kruppel-Like Factor 4 Positively Regulates Autoimmune
910 Arthritis in Mouse Models and Rheumatoid Arthritis in Patients via Modulating
911 Cell Survival and Inflammation Factors of Fibroblast-Like Synoviocyte. *Front*
912 *Immunol* **9**, 1339.
913 **Comazzetto, S., Shen, B. and Morrison, S. J.** (2021). Niches that regulate stem cells
914 and hematopoiesis in adult bone marrow. *Dev Cell* **56**, 1848-1860.
915 **Cumano, A., Berthault, C., Ramond, C., Petit, M., Golub, R., Bandeira, A. and**
916 **Pereira, P.** (2019). New Molecular Insights into Immune Cell Development.
917 *Annu Rev Immunol* **37**, 497-519.
918 **Curtis, A. M., Bellet, M. M., Sassone-Corsi, P. and O'Neill, L. A.** (2014). Circadian
919 clock proteins and immunity. *Immunity* **40**, 178-186.
920 **Decker, R. S., Um, H. B., Dyment, N. A., Cottingham, N., Usami, Y., Enomoto-**
921 **Iwamoto, M., Kronenberg, M. S., Maye, P., Rowe, D. W., Koyama, E., et al.**
922 (2017). Cell origin, volume and arrangement are drivers of articular cartilage
923 formation, morphogenesis and response to injury in mouse limbs. *Dev Biol* **426**,
924 56-68.

925 **Dhakal, M., Miller, M. M., Zaghouani, A. A., Sherman, M. P. and Zaghouani, H.**
926 (2015). Neonatal Basophils Stifle the Function of Early-Life Dendritic Cells To
927 Curtail Th1 Immunity in Newborn Mice. *J Immunol* **195**, 507-518.
928 **Di Rosa, F. and Gebhardt, T.** (2016). Bone Marrow T Cells and the Integrated
929 Functions of Recirculating and Tissue-Resident Memory T Cells. *Front*
930 *Immunol* **7**, 51.
931 **Ding, L. and Morrison, S. J.** (2013). Haematopoietic stem cells and early lymphoid
932 progenitors occupy distinct bone marrow niches. *Nature* **495**, 231-235.
933 **Ding, L., Saunders, T. L., Enikolopov, G. and Morrison, S. J.** (2012). Endothelial
934 and perivascular cells maintain haematopoietic stem cells. *Nature* **481**, 457-
935 462.
936 **Duchamp de Lageneste, O., Julien, A., Abou-Khalil, R., Frangi, G., Carvalho, C.,**
937 **Cagnard, N., Cordier, C., Conway, S. J. and Colnot, C.** (2018). Periosteum
938 contains skeletal stem cells with high bone regenerative potential controlled by
939 Periostin. *Nat Commun* **9**, 773.
940 **Efremova, M., Vento-Tormo, M., Teichmann, S. A. and Vento-Tormo, R.** (2020).
941 CellPhoneDB: inferring cell-cell communication from combined expression of
942 multi-subunit ligand-receptor complexes. *Nat Protoc* **15**, 1484-1506.
943 **Eschenbrenner, E., Jouannet, S., Clay, D., Chaker, J., Boucheix, C., Brou, C.,**
944 **Tomlinson, M. G., Charrin, S. and Rubinstein, E.** (2020). TspanC8
945 tetraspanins differentially regulate ADAM10 endocytosis and half-life. *Life Sci*
946 *Alliance* **3**.
947 **Ferreirinha, P., Pinheiro, R. G. R., Landry, J. J. M. and Alves, N. L.** (2022).
948 Identification of fibroblast progenitors in the developing mouse thymus.
949 *Development* **149**.
950 **Galea, G. L., Zein, M. R., Allen, S. and Francis-West, P.** (2021). Making and shaping
951 endochondral and intramembranous bones. *Dev Dyn* **250**, 414-449.
952 **Ghaleb, A. M. and Yang, V. W.** (2017). Kruppel-like factor 4 (KLF4): What we
953 currently know. *Gene* **611**, 27-37.
954 **Gomariz, A., Helbling, P. M., Isringhausen, S., Suessbier, U., Becker, A., Boss,**
955 **A., Nagasawa, T., Paul, G., Goksel, O., Szekely, G., et al.** (2018). Quantitative
956 spatial analysis of haematopoiesis-regulating stromal cells in the bone marrow
957 microenvironment by 3D microscopy. *Nat Commun* **9**, 2532.

958 **Gonzalez, M. J., Ruiz-Garcia, A., Monsalve, E. M., Sanchez-Prieto, R., Laborda,**
959 **J., Diaz-Guerra, M. J. and Ruiz-Hidalgo, M. J.** (2015). DLK1 is a novel
960 inflammatory inhibitor which interferes with NOTCH1 signaling in TLR-activated
961 murine macrophages. *Eur J Immunol* **45**, 2615-2627.
962 **Guarnerio, J., Coltella, N., Ala, U., Tonon, G., Pandolfi, P. P. and Bernardi, R.**
963 (2014). Bone marrow endosteal mesenchymal progenitors depend on HIF
964 factors for maintenance and regulation of hematopoiesis. *Stem Cell Reports* **2**,
965 794-809.
966 **Hai, T., Wolford, C. C. and Chang, Y. S.** (2010). ATF3, a hub of the cellular adaptive-
967 response network, in the pathogenesis of diseases: is modulation of
968 inflammation a unifying component? *Gene Expr* **15**, 1-11.
969 **Hallett, S. A., Ono, W. and Ono, N.** (2021). The hypertrophic chondrocyte: To be or
970 not to be. *Histol Histopathol* **36**, 1021-1036.
971 **Hao, Y., Hao, S., Andersen-Nissen, E., Mauck, W. M., 3rd, Zheng, S., Butler, A.,**
972 **Lee, M. J., Wilk, A. J., Darby, C., Zager, M., et al.** (2021). Integrated analysis
973 of multimodal single-cell data. *Cell* **184**, 3573-3587 e3529.
974 **Haraguchi, R., Kitazawa, R., Kohara, Y., Ikedo, A., Imai, Y. and Kitazawa, S.**
975 (2019). Recent Insights into Long Bone Development: Central Role of
976 Hedgehog Signaling Pathway in Regulating Growth Plate. *Int J Mol Sci* **20**.
977 **Helbling, P. M., Pineiro-Yanez, E., Gerosa, R., Boettcher, S., Al-Shahrour, F.,**
978 **Manz, M. G. and Nombela-Arrieta, C.** (2019). Global Transcriptomic Profiling
979 of the Bone Marrow Stromal Microenvironment during Postnatal Development,
980 Aging, and Inflammation. *Cell Rep* **29**, 3313-3330 e3314.
981 **Hillman, N. H., Kallapur, S. G. and Jobe, A. H.** (2012). Physiology of transition from
982 intrauterine to extrauterine life. *Clin Perinatol* **39**, 769-783.
983 **Ho, N. P. and Takizawa, H.** (2022). Inflammation Regulates Haematopoietic Stem
984 Cells and Their Niche. *Int J Mol Sci* **23**.
985 **Houlihan, D. D., Mabuchi, Y., Morikawa, S., Niibe, K., Araki, D., Suzuki, S., Okano,**
986 **H. and Matsuzaki, Y.** (2012). Isolation of mouse mesenchymal stem cells on
987 the basis of expression of Sca-1 and PDGFR-alpha. *Nat Protoc* **7**, 2103-2111.
988 **Hu, Y., Tan, L. J., Chen, X. D., Liu, Z., Min, S. S., Zeng, Q., Shen, H. and Deng, H.**
989 **W.** (2018). Identification of Novel Potentially Pleiotropic Variants Associated
990 With Osteoporosis and Obesity Using the cFDR Method. *J Clin Endocrinol*
991 *Metab* **103**, 125-138.

992 **Jeffery, E. C., Mann, T. L. A., Pool, J. A., Zhao, Z. and Morrison, S. J.** (2022). Bone
993 marrow and periosteal skeletal stem/progenitor cells make distinct contributions
994 to bone maintenance and repair. *Cell Stem Cell* **29**, 1547-1561 e1546.
995 **Jelinsky, S. A., Archambault, J., Li, L. and Seeherman, H.** (2010). Tendon-selective
996 genes identified from rat and human musculoskeletal tissues. *J Orthop Res* **28**,
997 289-297.
998 **Johnson, G. L., Masias, E. J. and Lehoczky, J. A.** (2020). Cellular Heterogeneity
999 and Lineage Restriction during Mouse Digit Tip Regeneration at Single-Cell
1000 Resolution. *Dev Cell* **52**, 525-540 e525.
1001 **Johnston, A. P.** (2017). Schwann cells: an emerging player in tissue regeneration.
1002 *Stem Cell Investig* **4**, 14.
1003 **Jung, Y. W., Kim, H. G., Perry, C. J. and Kaech, S. M.** (2016). CCR7 expression
1004 alters memory CD8 T-cell homeostasis by regulating occupancy in IL-7- and IL-
1005 15-dependent niches. *Proc Natl Acad Sci U S A* **113**, 8278-8283.
1006 **Kara, N., Xue, Y., Zhao, Z., Murphy, M. M., Comazzetto, S., Lesser, A., Du, L. and**
1007 **Morrison, S. J.** (2023). Endothelial and Leptin Receptor(+) cells promote the
1008 maintenance of stem cells and hematopoiesis in early postnatal murine bone
1009 marrow. *Dev Cell* **58**, 348-360 e346.
1010 **Kawata, M., Teramura, T., Ordoukhanian, P., Head, S. R., Natarajan, P.,**
1011 **Sundaresan, A., Olmer, M., Asahara, H. and Lotz, M. K.** (2022). Kruppel-like
1012 factor-4 and Kruppel-like factor-2 are important regulators of joint tissue cells
1013 and protect against tissue destruction and inflammation in osteoarthritis. *Ann*
1014 *Rheum Dis*.
1015 **Kemppainen, A. V., Finnila, M. A., Heikkinen, A., Haronen, H., Izzi, V., Kauppinen,**
1016 **S., Saarakkala, S., Pihlajaniemi, T. and Koivunen, J.** (2022). The CMS19
1017 disease model specifies a pivotal role for collagen XIII in bone homeostasis. *Sci*
1018 *Rep* **12**, 5866.
1019 **Knights, A. J., Yang, L., Shah, M., Norton, L. J., Green, G. S., Stout, E. S.,**
1020 **Vohralik, E. J., Crossley, M. and Quinlan, K. G. R.** (2020). Kruppel-like factor
1021 3 (KLF3) suppresses NF-kappaB-driven inflammation in mice. *J Biol Chem* **295**,
1022 6080-6091.
1023 **Komori, T.** (2022). Whole Aspect of Runx2 Functions in Skeletal Development. *Int J*
1024 *Mol Sci* **23**.

1025 **Korsunsky, I., Millard, N., Fan, J., Slowikowski, K., Zhang, F., Wei, K., Baglaenko,**
1026 **Y., Brenner, M., Loh, P. R. and Raychaudhuri, S.** (2019). Fast, sensitive and
1027 accurate integration of single-cell data with Harmony. *Nat Methods* **16**, 1289-
1028 1296.
1029 **Kwon, J. W., Kwon, H. K., Shin, H. J., Choi, Y. M., Anwar, M. A. and Choi, S.**
1030 (2015). Activating transcription factor 3 represses inflammatory responses by
1031 binding to the p65 subunit of NF-kappaB. *Sci Rep* **5**, 14470.
1032 **Lavaert, M., Liang, K. L., Vandamme, N., Park, J. E., Roels, J., Kowalczyk, M. S.,**
1033 **Li, B., Ashenberg, O., Tabaka, M., Dionne, D., et al.** (2020). Integrated
1034 scRNA-Seq Identifies Human Postnatal Thymus Seeding Progenitors and
1035 Regulatory Dynamics of Differentiating Immature Thymocytes. *Immunity* **52**,
1036 1088-1104 e1086.
1037 **Lee, P. Y., Wang, J. X., Parisini, E., Dascher, C. C. and Nigrovic, P. A.** (2013). Ly6
1038 family proteins in neutrophil biology. *J Leukoc Biol* **94**, 585-594.
1039 **Li, C., Yu, L., Mai, C., Mu, T. and Zeng, Y.** (2021). KLF4 down-regulation resulting
1040 from TLR4 promotion of ERK1/2 phosphorylation underpins inflammatory
1041 response in sepsis. *J Cell Mol Med* **25**, 2013-2024.
1042 **Li, Q., Xu, R., Lei, K. and Yuan, Q.** (2022a). Insights into skeletal stem cells. *Bone*
1043 *Res* **10**, 61.
1044 **Li, Z., Bowers, E., Zhu, J., Yu, H., Hardij, J., Bagchi, D. P., Mori, H., Lewis, K. T.,**
1045 **Granger, K., Schill, R. L., et al.** (2022b). Lipolysis of bone marrow adipocytes
1046 is required to fuel bone and the marrow niche during energy deficits. *Elife* **11**.
1047 **Liao, X., Sharma, N., Kapadia, F., Zhou, G., Lu, Y., Hong, H., Paruchuri, K.,**
1048 **Mahabeleshwar, G. H., Dalmas, E., Venteclef, N., et al.** (2011). Kruppel-like
1049 factor 4 regulates macrophage polarization. *J Clin Invest* **121**, 2736-2749.
1050 **Liggins, G. C.** (1994). The role of cortisol in preparing the fetus for birth. *Reprod Fertil*
1051 *Dev* **6**, 141-150.
1052 **Lima, I. L. A., Silva, J. M. D., Rodrigues, L. F. D., Madureira, D. F., Fonseca, A. C.,**
1053 **Garlet, G. P., Teixeira, M. M., Russo, R. C., Fukada, S. Y. and Silva, T. A. D.**
1054 (2017). Contribution of atypical chemokine receptor 2/ackr2 in bone
1055 remodeling. *Bone* **101**, 113-122.
1056 **Lin, T. Y., Gerber, T., Taniguchi-Sugiura, Y., Murawala, P., Hermann, S., Grosser,**
1057 **L., Shibata, E., Treutlein, B. and Tanaka, E. M.** (2021). Fibroblast

1058 dedifferentiation as a determinant of successful regeneration. *Dev Cell* **56**,
1059 1541-1551 e1546.
1060 **Liu, C., Lan, Y., Liu, B., Zhang, H. and Hu, H.** (2021). T Cell Development: Old Tales
1061 Retold By Single-Cell RNA Sequencing. *Trends Immunol* **42**, 165-175.
1062 **Liu, H., Zhang, C., Zhu, S., Lu, P., Zhu, T., Gong, X., Zhang, Z., Hu, J., Yin, Z.,**
1063 **Heng, B. C., et al.** (2015). Mohawk promotes the tenogenesis of mesenchymal
1064 stem cells through activation of the TGFbeta signaling pathway. *Stem Cells* **33**,
1065 443-455.
1066 **Liu, H., Zhu, Y., Gao, Y., Qi, D., Zhao, L., Zhao, L., Liu, C., Tao, T., Zhou, C., Sun,**
1067 **X., et al.** (2020). NR1D1 modulates synovial inflammation and bone destruction
1068 in rheumatoid arthritis. *Cell Death Dis* **11**, 129.
1069 **Liu, Y., Chen, Q., Jeong, H. W., Koh, B. I., Watson, E. C., Xu, C., Stehling, M.,**
1070 **Zhou, B. and Adams, R. H.** (2022). A specialized bone marrow
1071 microenvironment for fetal haematopoiesis. *Nat Commun* **13**, 1327.
1072 **Long, F. and Ornitz, D. M.** (2013). Development of the endochondral skeleton. *Cold*
1073 *Spring Harb Perspect Biol* **5**, a008334.
1074 **Long, K. R. and Huttner, W. B.** (2019). How the extracellular matrix shapes neural
1075 development. *Open Biol* **9**, 180216.
1076 **Luecken, M. D., Buttner, M., Chaichoompu, K., Danese, A., Interlandi, M., Mueller,**
1077 **M. F., Strobl, D. C., Zappia, L., Dugas, M., Colome-Tatche, M., et al.** (2022).
1078 Benchmarking atlas-level data integration in single-cell genomics. *Nat Methods*
1079 **19**, 41-50.
1080 **Luo, Y., Acevedo, D., Banos, N., Pluma, A., Castellanos-Moreira, R., Moreno, E.,**
1081 **Rodriguez-Garcia, S., Deya-Martinez, A., Garcia-Garcia, A., Quesada-**
1082 **Masachs, E., et al.** (2023). Expected impact of immunomodulatory agents
1083 during pregnancy: A newborn's perspective. *Pediatr Allergy Immunol* **34**,
1084 e13911.
1085 **Mallo, M.** (2018). Reassessing the Role of Hox Genes during Vertebrate Development
1086 and Evolution. *Trends Genet* **34**, 209-217.
1087 **Matsushita, Y., Nagata, M., Kozloff, K. M., Welch, J. D., Mizuhashi, K.,**
1088 **Tokavanich, N., Hallett, S. A., Link, D. C., Nagasawa, T., Ono, W., et al.**
1089 (2020). A Wnt-mediated transformation of the bone marrow stromal cell identity
1090 orchestrates skeletal regeneration. *Nat Commun* **11**, 332.

1091 **Matsushita, Y., Ono, W. and Ono, N.** (2021). Bone regeneration via skeletal cell
1092 lineage plasticity: All hands mobilized for emergencies: Quiescent mature
1093 skeletal cells can be activated in response to injury and robustly participate in
1094 bone regeneration through cellular plasticity. *Bioessays* **43**, e2000202.
1095 **Matthews, B. G., Novak, S., Sbrana, F. V., Funnell, J. L., Cao, Y., Buckels, E. J.,**
1096 **Grcevic, D. and Kalajzic, I.** (2021). Heterogeneity of murine periosteum
1097 progenitors involved in fracture healing. *Elife* **10**.
1098 **McGinnis, C. S., Murrow, L. M. and Gartner, Z. J.** (2019). DoubletFinder: Doublet
1099 Detection in Single-Cell RNA Sequencing Data Using Artificial Nearest
1100 Neighbors. *Cell Syst* **8**, 329-337 e324.
1101 **Milet, C. and Duprez, D.** (2015). The Mkx homeoprotein promotes tenogenesis in
1102 stem cells and improves tendon repair. *Ann Transl Med* **3**, S33.
1103 **Mizoguchi, T., Pinho, S., Ahmed, J., Kunisaki, Y., Hanoun, M., Mendelson, A.,**
1104 **Ono, N., Kronenberg, H. M. and Frenette, P. S.** (2014). Osterix marks distinct
1105 waves of primitive and definitive stromal progenitors during bone marrow
1106 development. *Dev Cell* **29**, 340-349.
1107 **Mizuno, S., Yoda, M., Kimura, T., Shimoda, M., Akiyama, H., Chiba, K., Nakamura,**
1108 **M. and Horiuchi, K.** (2020). ADAM10 is indispensable for longitudinal bone
1109 growth in mice. *Bone* **134**, 115273.
1110 **Mo, C., Guo, J., Qin, J., Zhang, X., Sun, Y., Wei, H., Cao, D., Zhang, Y., Zhao, C.,**
1111 **Xiong, Y., et al.** (2022). Single-cell transcriptomics of LepR-positive skeletal
1112 cells reveals heterogeneous stress-dependent stem and progenitor pools.
1113 *EMBO J* **41**, e108415.
1114 **Moore, F., Santin, I., Nogueira, T. C., Gurzov, E. N., Marselli, L., Marchetti, P. and**
1115 **Eizirik, D. L.** (2012). The transcription factor C/EBP delta has anti-apoptotic
1116 and anti-inflammatory roles in pancreatic beta cells. *PLoS One* **7**, e31062.
1117 **Morikawa, S., Mabuchi, Y., Kubota, Y., Nagai, Y., Niibe, K., Hiratsu, E., Suzuki, S.,**
1118 **Miyauchi-Hara, C., Nagoshi, N., Sunabori, T., et al.** (2009). Prospective
1119 identification, isolation, and systemic transplantation of multipotent
1120 mesenchymal stem cells in murine bone marrow. *J Exp Med* **206**, 2483-2496.
1121 **Morrison, S. J. and Scadden, D. T.** (2014). The bone marrow niche for
1122 haematopoietic stem cells. *Nature* **505**, 327-334.
1123 **Morton, S. U. and Brodsky, D.** (2016). Fetal Physiology and the Transition to
1124 Extrauterine Life. *Clin Perinatol* **43**, 395-407.

1125 **Mucientes, A., Herranz, E., Moro, E., Lajas, C., Candelas, G., Fernandez-**
1126 **Gutierrez, B. and Lamas, J. R.** (2018). Differential Expression of HOX Genes
1127 in Mesenchymal Stem Cells from Osteoarthritic Patients Is Independent of Their
1128 Promoter Methylation. *Cells* **7**.
1129 **Murchison, N. D., Price, B. A., Conner, D. A., Keene, D. R., Olson, E. N., Tabin, C.**
1130 **J. and Schweitzer, R.** (2007). Regulation of tendon differentiation by scleraxis
1131 distinguishes force-transmitting tendons from muscle-anchoring tendons.
1132 *Development* **134**, 2697-2708.
1133 **Newton, P. T., Li, L., Zhou, B., Schweingruber, C., Hovorakova, M., Xie, M., Sun,**
1134 **X., Sandhow, L., Artemov, A. V., Ivashkin, E., et al.** (2019). A radical switch
1135 in clonality reveals a stem cell niche in the epiphyseal growth plate. *Nature* **567**,
1136 234-238.
1137 **Nusspaumer, G., Jaiswal, S., Barbero, A., Reinhardt, R., Ishay Ronen, D.,**
1138 **Haumer, A., Lufkin, T., Martin, I. and Zeller, R.** (2017). Ontogenic
1139 Identification and Analysis of Mesenchymal Stromal Cell Populations during
1140 Mouse Limb and Long Bone Development. *Stem Cell Reports* **9**, 1124-1138.
1141 **Omatsu, Y., Sugiyama, T., Kohara, H., Kondoh, G., Fujii, N., Kohno, K. and**
1142 **Nagasawa, T.** (2010). The essential functions of adipo-osteogenic progenitors
1143 as the hematopoietic stem and progenitor cell niche. *Immunity* **33**, 387-399.
1144 **Ortinau, L. C., Wang, H., Lei, K., Deveza, L., Jeong, Y., Hara, Y., Grafe, I.,**
1145 **Rosenfeld, S. B., Lee, D., Lee, B., et al.** (2019). Identification of Functionally
1146 Distinct Mx1+alphaSMA+ Periosteal Skeletal Stem Cells. *Cell Stem Cell* **25**,
1147 784-796 e785.
1148 **Pacifici, M., Koyama, E., Iwamoto, M. and Gentili, C.** (2000). Development of
1149 articular cartilage: what do we know about it and how may it occur? *Connect*
1150 *Tissue Res* **41**, 175-184.
1151 **Pai, P. and Sukumar, S.** (2020). HOX genes and the NF-kappaB pathway: A
1152 convergence of developmental biology, inflammation and cancer biology.
1153 *Biochim Biophys Acta Rev Cancer* **1874**, 188450.
1154 **Perrin, S., Wotawa, C.-A., Luka, M., Coulpier, F., Masson, C., Ménager, M. and**
1155 **Colnot, C.** (2023). Periosteal response to bone fracture at single nuclei
1156 resolution. *bioRxiv*, 2023.2006.2023.546220.
1157 **Ranzoni, A. M., Tangherloni, A., Berest, I., Riva, S. G., Myers, B., Strzelecka, P.**
1158 **M., Xu, J., Panada, E., Mohorianu, I., Zaugg, J. B., et al.** (2021). Integrative

1159 Single-Cell RNA-Seq and ATAC-Seq Analysis of Human Developmental
1160 Hematopoiesis. *Cell Stem Cell* **28**, 472-487 e477.
1161 **Rao, J., Chal, J., Marchianò, F., Wang, C.-H., Tanoury, Z. A., Gapon, S., Djeffal,**
1162 **Y., Mayeuf-Louchart, A., Glass, I., Sefton, E. M., et al.** (2022). Reconstructing
1163 human Brown Fat developmental trajectory in vitro. *bioRxiv*,
1164 2022.2006.2001.494355.
1165 **Rebelo, A. P., Cortese, A., Abraham, A., Eshed-Eisenbach, Y., Shner, G.,**
1166 **Vainshtein, A., Buglo, E., Camarena, V., Gaidosh, G., Shiekhattar, R., et al.**
1167 (2021). A CADM3 variant causes Charcot-Marie-Tooth disease with marked
1168 upper limb involvement. *Brain* **144**, 1197-1213.
1169 **Rees, S. G., Waggett, A. D., Kerr, B. C., Probert, J., Gealy, E. C., Dent, C. M.,**
1170 **Caterson, B. and Hughes, C. E.** (2009). Immunolocalisation and expression
1171 of keratocan in tendon. *Osteoarthritis Cartilage* **17**, 276-279.
1172 **Rothenberg, E. V.** (2021). Single-cell insights into the hematopoietic generation of T-
1173 lymphocyte precursors in mouse and human. *Exp Hematol* **95**, 1-12.
1174 **Rustenhoven, J., Scotter, E. L., Jansson, D., Kho, D. T., Oldfield, R. L., Bergin, P.**
1175 **S., Mee, E. W., Faull, R. L., Curtis, M. A., Graham, S. E., et al.** (2015). An
1176 anti-inflammatory role for C/EBPdelta in human brain pericytes. *Sci Rep* **5**,
1177 12132.
1178 **Rux, D. R., Song, J. Y., Swinehart, I. T., Pineault, K. M., Schlientz, A. J., Trulik, K.**
1179 **G., Goldstein, S. A., Kozloff, K. M., Lucas, D. and Wellik, D. M.** (2016).
1180 Regionally Restricted Hox Function in Adult Bone Marrow Multipotent
1181 Mesenchymal Stem/Stromal Cells. *Dev Cell* **39**, 653-666.
1182 **Sakaguchi, S., Takahashi, T. and Nishizuka, Y.** (1982). Study on cellular events in
1183 post-thymectomy autoimmune oophoritis in mice. II. Requirement of Lyt-1 cells
1184 in normal female mice for the prevention of oophoritis. *J Exp Med* **156**, 1577-
1185 1586.
1186 **Sanidad, K. Z. and Zeng, M. Y.** (2020). Neonatal gut microbiome and immunity. *Curr*
1187 *Opin Microbiol* **56**, 30-37.
1188 **Scheiermann, C., Kunisaki, Y. and Frenette, P. S.** (2013). Circadian control of the
1189 immune system. *Nat Rev Immunol* **13**, 190-198.
1190 **Seale, P., Bjork, B., Yang, W., Kajimura, S., Chin, S., Kuang, S., Scime, A.,**
1191 **Devarakonda, S., Conroe, H. M., Erdjument-Bromage, H., et al.** (2008).
1192 PRDM16 controls a brown fat/skeletal muscle switch. *Nature* **454**, 961-967.

1193 **Severe, N., Karabacak, N. M., Gustafsson, K., Baryawno, N., Courties, G., Kfoury,**
1194 **Y., Kokkaliaris, K. D., Rhee, C., Lee, D., Scadden, E. W., et al.** (2019). Stress-
1195 Induced Changes in Bone Marrow Stromal Cell Populations Revealed through
1196 Single-Cell Protein Expression Mapping. *Cell Stem Cell* **25**, 570-583 e577.
1197 **Shan, Q., Li, X., Chen, X., Zeng, Z., Zhu, S., Gai, K., Peng, W. and Xue, H. H.** (2021).
1198 Tcf1 and Lef1 provide constant supervision to mature CD8(+) T cell identity and
1199 function by organizing genomic architecture. *Nat Commun* **12**, 5863.
1200 **Shay, D. A., Welly, R. J., Givan, S. A., Bivens, N., Kanaley, J., Marshall, B. L.,**
1201 **Lubahn, D. B., Rosenfeld, C. S. and Vieira-Potter, V. J.** (2020). Changes in
1202 nucleus accumbens gene expression accompany sex-specific suppression of
1203 spontaneous physical activity in aromatase knockout mice. *Horm Behav* **121**,
1204 104719.
1205 **Shu, H. S., Liu, Y. L., Tang, X. T., Zhang, X. S., Zhou, B., Zou, W. and Zhou, B. O.**
1206 (2021). Tracing the skeletal progenitor transition during postnatal bone
1207 formation. *Cell Stem Cell* **28**, 2122-2136 e2123.
1208 **Shukunami, C., Takimoto, A., Nishizaki, Y., Yoshimoto, Y., Tanaka, S., Miura, S.,**
1209 **Watanabe, H., Sakuma, T., Yamamoto, T., Kondoh, G., et al.** (2018).
1210 Scleraxis is a transcriptional activator that regulates the expression of
1211 Tenomodulin, a marker of mature tenocytes and ligamentocytes. *Sci Rep* **8**,
1212 3155.
1213 **Stone, A., Rand, E., Thornes, G., Kay, A., Barnes, A., Hitchcock, I. and Genever,**
1214 **P.** (2023). Extracellular matrices of bone marrow stroma regulate cell
1215 phenotype and contribute to distinct stromal niches in vivo. *bioRxiv*,
1216 2023.2001.2019.524473.
1217 **Storer, M. A., Mahmud, N., Karamboulas, K., Borrett, M. J., Yuzwa, S. A., Gont,**
1218 **A., Androschuk, A., Sefton, M. V., Kaplan, D. R. and Miller, F. D.** (2020).
1219 Acquisition of a Unique Mesenchymal Precursor-like Blastema State Underlies
1220 Successful Adult Mammalian Digit Tip Regeneration. *Dev Cell* **52**, 509-524
1221 e509.
1222 **Sugiyama, T., Kohara, H., Noda, M. and Nagasawa, T.** (2006). Maintenance of the
1223 hematopoietic stem cell pool by CXCL12-CXCR4 chemokine signaling in bone
1224 marrow stromal cell niches. *Immunity* **25**, 977-988.
1225 **Tikhonova, A. N., Dolgalev, I., Hu, H., Sivaraj, K. K., Hoxha, E., Cuesta-**
1226 **Dominguez, A., Pinho, S., Akhmetzyanova, I., Gao, J., Witkowski, M., et al.**

1227 (2019). The bone marrow microenvironment at single-cell resolution. *Nature*
1228 **569**, 222-228.
1229 **Triana, S., Vonficht, D., Jopp-Saile, L., Raffel, S., Lutz, R., Leonce, D., Antes, M.,**
1230 **Hernandez-Malmierca, P., Ordonez-Rueda, D., Ramasz, B., et al.** (2021).
1231 Single-cell proteo-genomic reference maps of the hematopoietic system enable
1232 the purification and massive profiling of precisely defined cell states. *Nat*
1233 *Immunol* **22**, 1577-1589.
1234 **Van de Sande, B., Flerin, C., Davie, K., De Waegeneer, M., Hulselmans, G., Aibar,**
1235 **S., Seurinck, R., Saelens, W., Cannoodt, R., Rouchon, Q., et al.** (2020). A
1236 scalable SCENIC workflow for single-cell gene regulatory network analysis. *Nat*
1237 *Protoc* **15**, 2247-2276.
1238 **Van Nguyen, T. T., Vu, V. V. and Pham, P. V.** (2020). Transcriptional Factors of
1239 Thermogenic Adipocyte Development and Generation of Brown and Beige
1240 Adipocytes From Stem Cells. *Stem Cell Rev Rep* **16**, 876-892.
1241 **Wessells, J., Baer, M., Young, H. A., Claudio, E., Brown, K., Siebenlist, U. and**
1242 **Johnson, P. F.** (2004). BCL-3 and NF-kappaB p50 attenuate
1243 lipopolysaccharide-induced inflammatory responses in macrophages. *J Biol*
1244 *Chem* **279**, 49995-50003.
1245 **Wolock, S. L., Krishnan, I., Tenen, D. E., Matkins, V., Camacho, V., Patel, S.,**
1246 **Agarwal, P., Bhatia, R., Tenen, D. G., Klein, A. M., et al.** (2019). Mapping
1247 Distinct Bone Marrow Niche Populations and Their Differentiation Paths. *Cell*
1248 *Rep* **28**, 302-311 e305.
1249 **Yang, L., Tsang, K. Y., Tang, H. C., Chan, D. and Cheah, K. S.** (2014). Hypertrophic
1250 chondrocytes can become osteoblasts and osteocytes in endochondral bone
1251 formation. *Proc Natl Acad Sci U S A* **111**, 12097-12102.
1252 **Yang, S., Fujikado, N., Kolodin, D., Benoist, C. and Mathis, D.** (2015). Immune
1253 tolerance. Regulatory T cells generated early in life play a distinct role in
1254 maintaining self-tolerance. *Science* **348**, 589-594.
1255 **Ylonen, R., Kyronlahti, T., Sund, M., Ilves, M., Lehenkari, P., Tuukkanen, J. and**
1256 **Pihlajaniemi, T.** (2005). Type XIII collagen strongly affects bone formation in
1257 transgenic mice. *J Bone Miner Res* **20**, 1381-1393.
1258 **Zeng, Y., Liu, C., Gong, Y., Bai, Z., Hou, S., He, J., Bian, Z., Li, Z., Ni, Y., Yan, J.,**
1259 **et al.** (2019). Single-Cell RNA Sequencing Resolves Spatiotemporal

Development of Pre-thymic Lymphoid Progenitors and Thymus Organogenesis in Human Embryos. *Immunity* **51**, 930-948 e936.

Zhang, Y., Kao, W. W., Hayashi, Y., Zhang, L., Call, M., Dong, F., Yuan, Y., Zhang, J., Wang, Y. C., Yuka, O., et al. (2017). Generation and Characterization of a Novel Mouse Line, Keratocan-rtTA (KeraRT), for Corneal Stroma and Tendon Research. *Invest Ophthalmol Vis Sci* **58**, 4800-4808.

Zhou, X., von der Mark, K., Henry, S., Norton, W., Adams, H. and de Crombrugghe, B. (2014). Chondrocytes transdifferentiate into osteoblasts in endochondral bone during development, postnatal growth and fracture healing in mice. *PLoS Genet* **10**, e1004820.

Zieba, J. T., Chen, Y. T., Lee, B. H. and Bae, Y. (2020). Notch Signaling in Skeletal Development, Homeostasis and Pathogenesis. *Biomolecules* **10**.

FIGURE 1

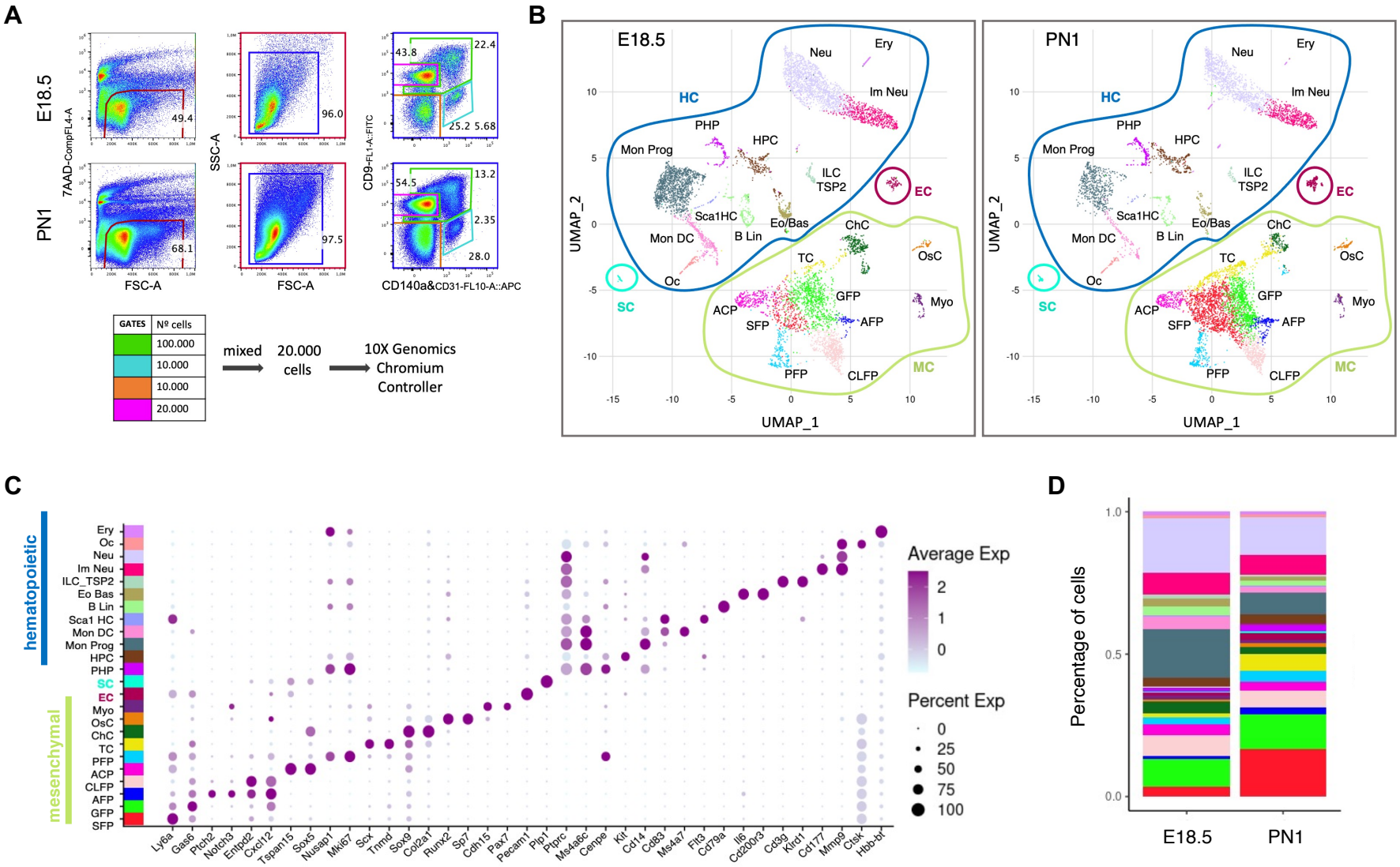
A
E18.5
PN1
7AAD-CompFL4-A
FSC-A
SSC-A
CD9-FL1-A::FITC
CD140a&CD31-FL10-A::APC
49.4
68.1
96.0
97.5
43.8
22.4
25.2
5.68
54.5
13.2
2.35
28.0
GATES
Nº cells
100.000
10.000
10.000
20.000
mixed
20.000 cells
10X Genomics Chromium Controller
B
E18.5
PN1
UMAP_1
UMAP_2
HC
SC
EC
MC
Neu
Ery
Im Neu
PHP
HPC
Mon Prog
ILC TSP2
Sca1HC
Eo/Bas
Mon DC
B Lin
ChC
TC
OsC
Oc
GFP
Myo
ACP
AFP
SFP
PFP
CLFP
C
hematopoietic
mesenchymal
Ery
Oc
Neu
Im Neu
ILC_TSP2
Eo Bas
B Lin
Sca1 HC
Mon DC
Mon Prog
HPC
PHP
SC
EC
Myo
OsC
ChC
TC
PFP
ACP
CLFP
AFP
GFP
SFP
Ly6a
Gas6
Ptch2
Notch3
Entpd2
Cxcl12
Tspan15
Sox5
Nusap1
Mki67
Scx
Tnmd
Sox9
Col2a1
Runx2
Sp7
Cdh15
Pax7
Pecam1
Plp1
Ptprc
Ms4a6c
Cenpe
Kit
Cd14
Cd83
Ms4a7
Flt3
Cd79a
Il6
Cd200r3
Cd3g
Klrd1
Cd177
Mmp9
Ctsk
Hbb-bt
Average Exp
2
1
0
Percent Exp
0
25
50
75
100
D
Percentage of cells
1.0
0.5
0.0
E18.5
PN1

FIGURE 2

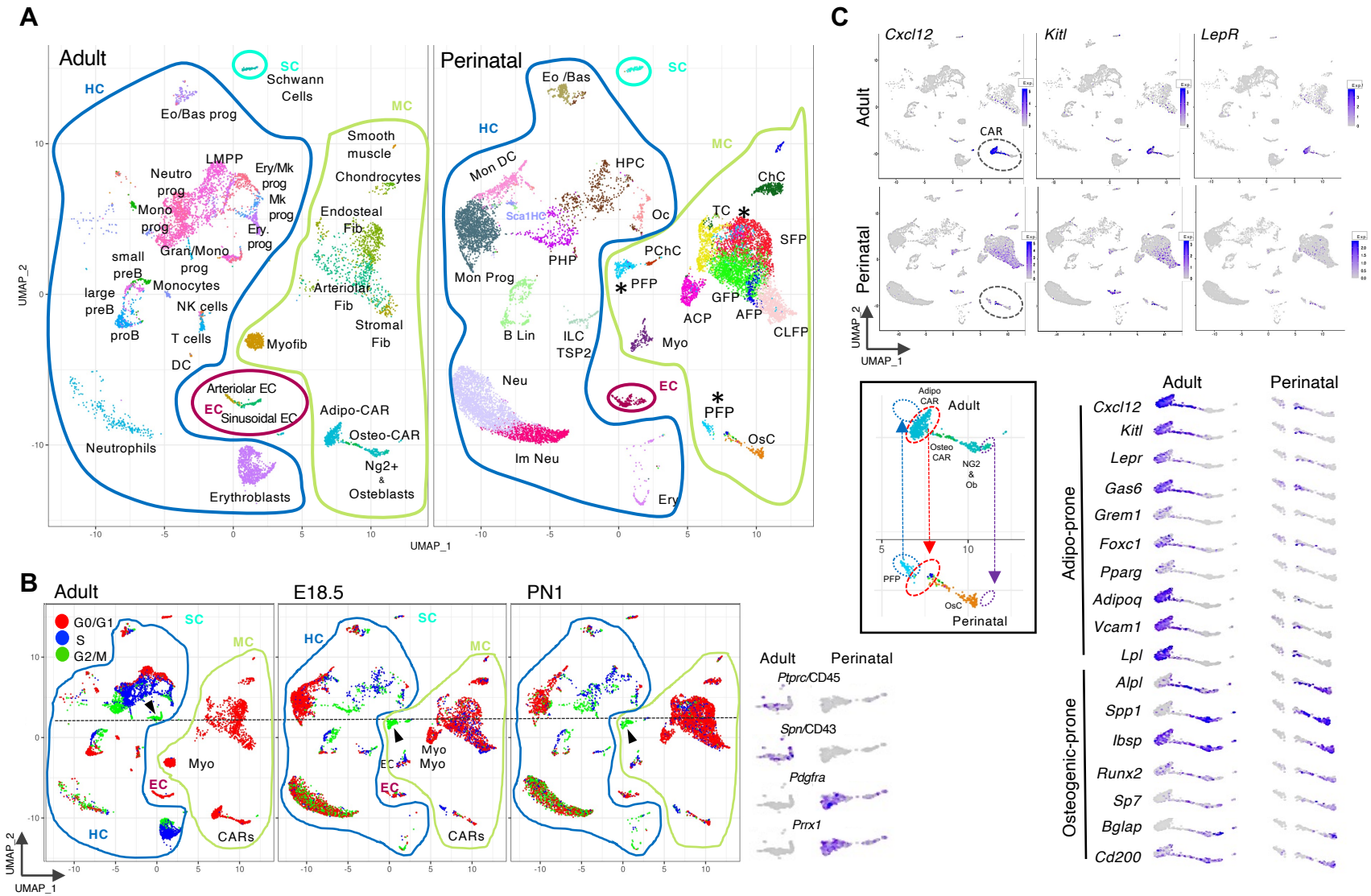
A
Adult
Perinatal
HC
SC
MC
Schwann Cells
Eo/Bas prog
Eo /Bas
Smooth muscle
Chondrocytes
Endosteal Fib
Arteriolar Fib
Stromal Fib
Myofib
Adipo-CAR
Osteo-CAR
Ng2+ & Osteoblasts
Arteriolar EC
Sinusoidal EC
EC
Erythroblasts
Neutrophils
DC
T cells
NK cells
Monocytes
Gran/Mono prog
small preB
large preB
proB
Mono prog
Neutro prog
LMPP
Ery/Mk prog
Mk prog
Ery. prog
Mon DC
Sca1HC
Mon Prog
HPC
PHP
Oc
PChC
PFP
B Lin
ILC TSP2
Neu
Im Neu
Myo
Ery
ChC
TC
SFP
GFP
AFP
ACP
CLFP
OsC
UMAP_1
UMAP_2
B
Adult
E18.5
PN1
G0/G1
S
G2/M
Myo
CARs
C
Cxcl12
Kitl
LepR
CAR
Adipo CAR
Osteo CAR
NG2 & Ob
Ptprc/CD45
Spn/CD43
Pdgfra
Prrx1
Adipo-prone
Osteogenic-prone
Alpl
Spp1
Ibsp
Runx2
Sp7
Bglap
Cd200
Lepr
Gas6
Grem1
Foxc1
Pparg
Adipoq
Vcam1
Lpl

FIGURE 3

A

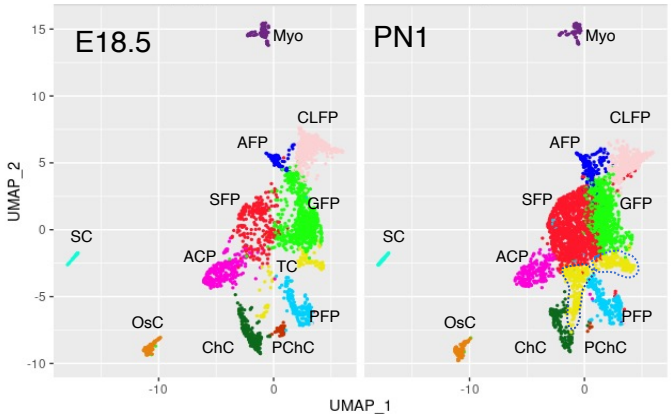
E18.5
PN1
Myo
CLFP
AFP
SFP
GFP
SC
ACP
TC
OsC
PFP
ChC
PChC
UMAP_2
UMAP_1

B

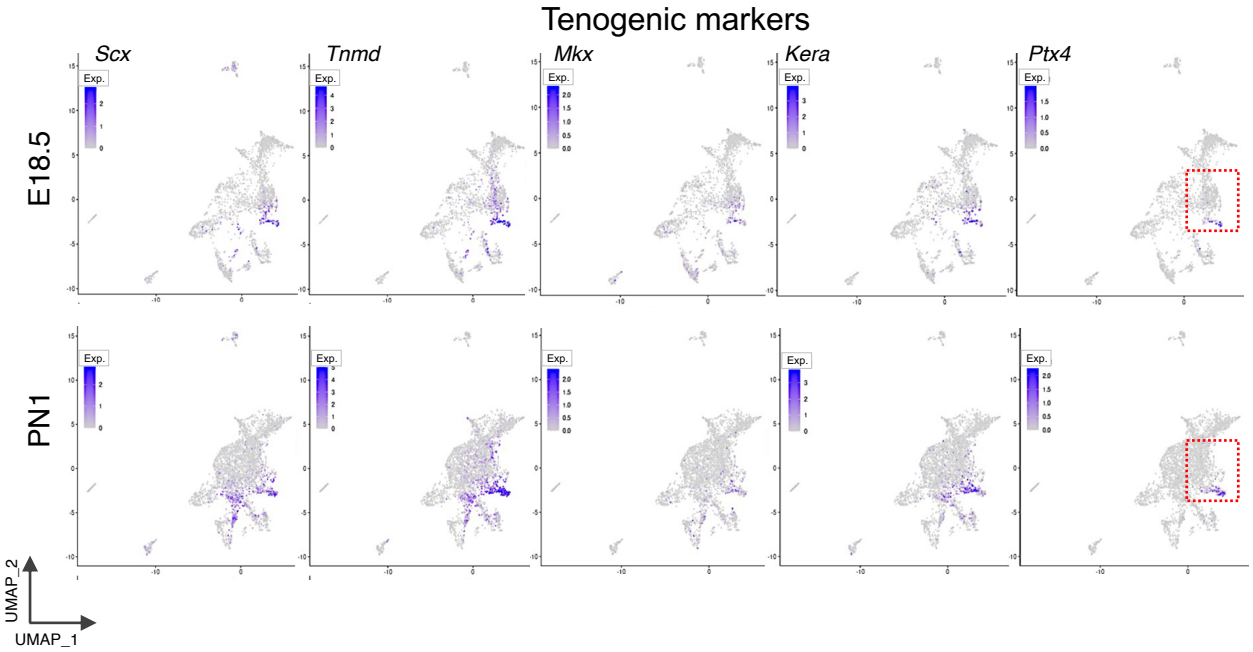
Tenogenic markers
Scx
Tnmd
Mkx
Kera
Ptx4
E18.5
PN1
Exp.
UMAP_2
UMAP_1

C

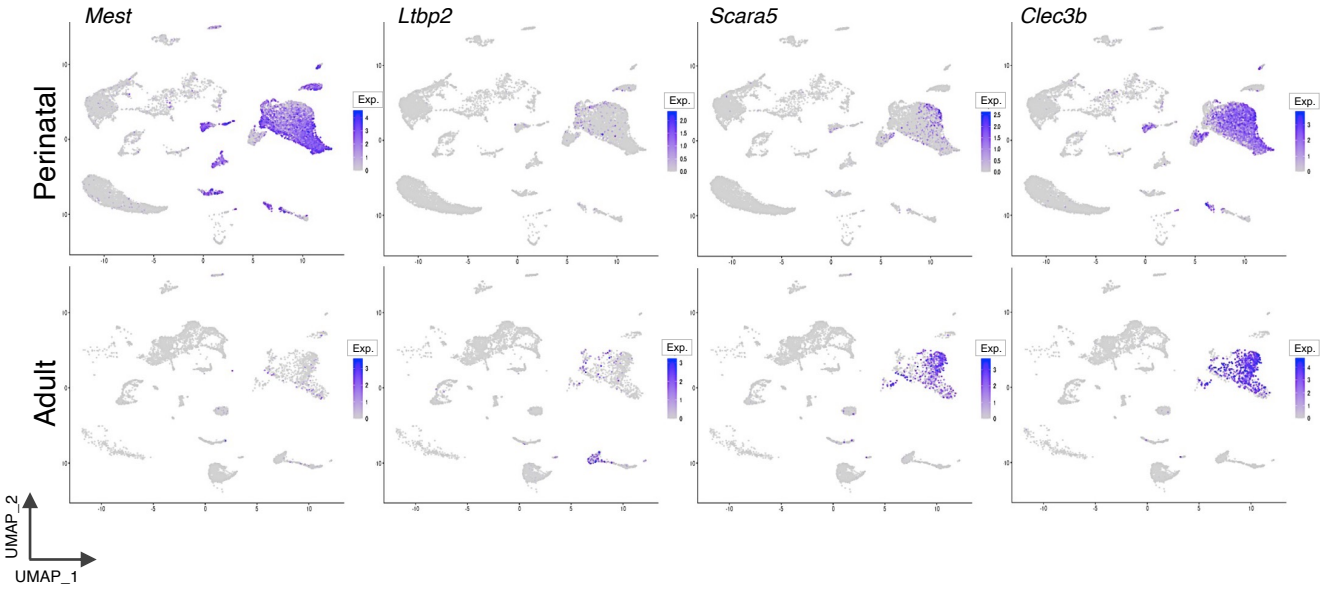
Blastema-like markers
Mest
Ltbp2
Scara5
Clec3b
Perinatal
Adult
Exp.
UMAP_2
UMAP_1

FIGURE 4

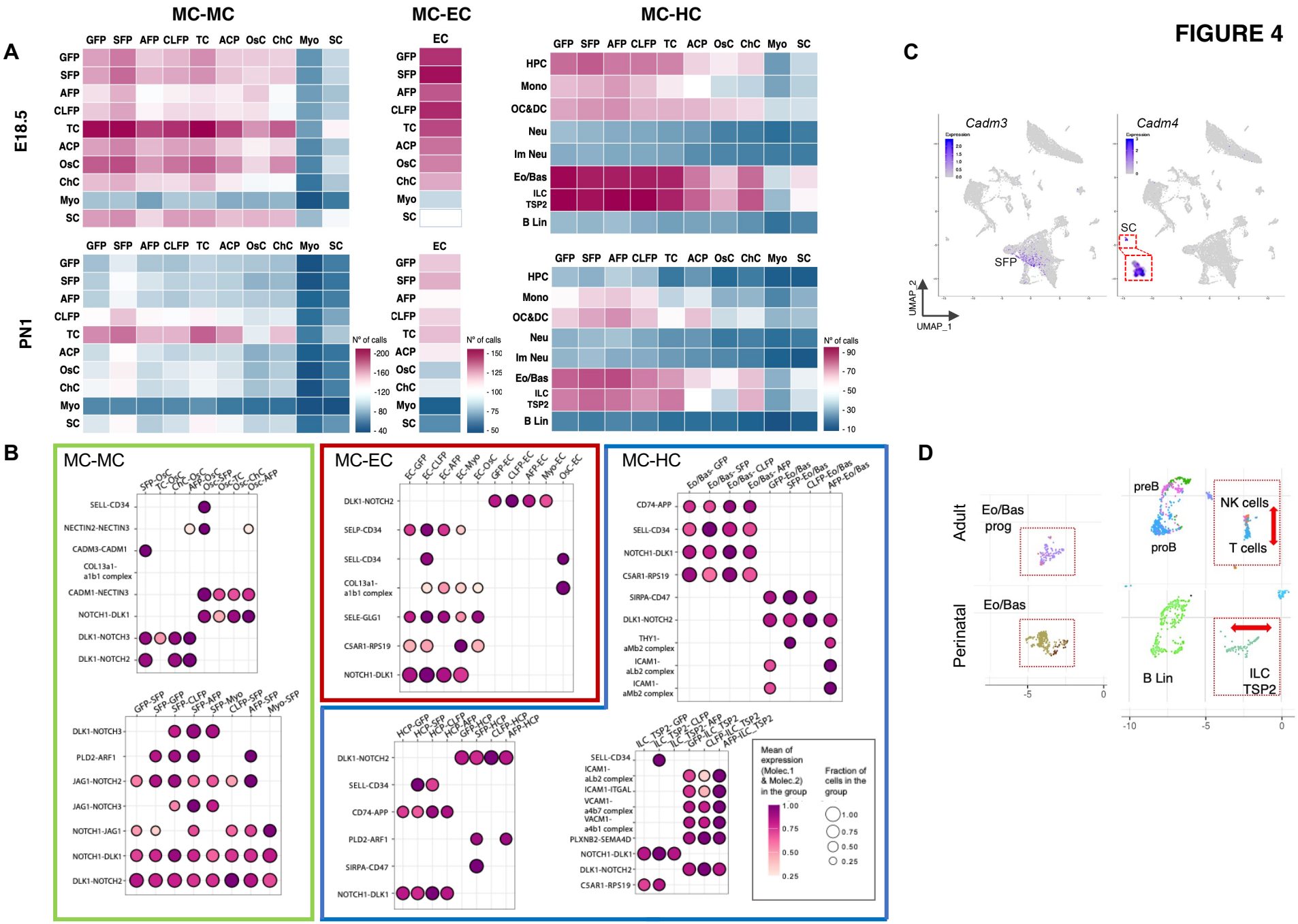
A
MC-MC
MC-EC
MC-HC
E18.5
PN1
GFP SFP AFP CLFP TC ACP OsC ChC Myo SC
EC
HPC
Mono
OC&DC
Neu
Im Neu
Eo/Bas
ILC TSP2
B Lin
N° of calls
B
MC-MC
MC-EC
MC-HC
C
Cadm3
Cadm4
SFP
SC
UMAP_2
UMAP_1
D
Adult
Perinatal
Eo/Bas prog
Eo/Bas
preB
proB
NK cells
T cells
B Lin
ILC TSP2
Mean of expression (Molec.1 & Molec.2) in the group
Fraction of cells in the group

FIGURE 5

A

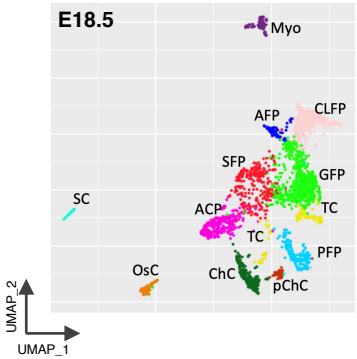

Regulons (+) controlling *genes*

Klf3	*Atf3*	*Nfkb1*	*Cebpd*
Klf3 (+)	**Atf3(+)**	**Nfkb1 (+)**	**Cebpd(+)**
Hoxa7 (+)	**Cebpd (+)**	**Atf3 (+)**	Gata6 (+)
Hoxd9(+)	Gsc (+)	Bcl3 (+)	Irf1 (+)
Lhx9 (+)	Erg1 (+)	Erg3 (+)	
Fosl1 (+)	Fosl1 (+)	Fosl1 (+)	
Foxc1 (+)	Cebpb (+)	Cebpb (+)	Tcf7l2(+)
	Gata6 (+)	Irf8 (+)	Meox1(+)
	Jun (+)	Spi1 (+)	Jun (+)
	Rel (+)	Rel (+)	
	Nfil3 (+)		
	Fosb (+)		
	Maff (+)		

B

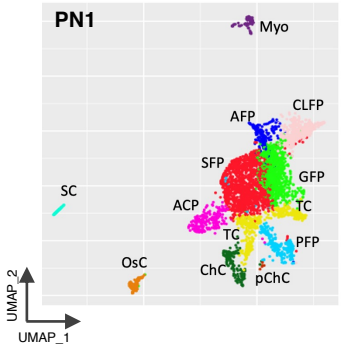

Regulons (+) controlling *genes*

Klf4	*Atf3*	*Nfkb1*	*Cebpd*	*Nr1d1*
Klf4 (+)	**Atf3 (+)**	**Nfkb1 (+)**	**Cebpd(+)**	**Nr1d1 (+)**
Atf3 (+)	**Cebpd (+)**	**Atf3 (+)**		
Barx1 (+)	Barx1 (+)	Bcl3 (+)	Tcf7l2(+)	
Fosb (+)	Fosb (+)	Maff (+)	Irf1(+)	Irf8 (+)
Fosl1 (+)	Fosl1 (+)			Fosl1(+)
Foxc1 (+)	Foxc1 (+)	Spi1 (+)	Spi1(+)	
Foxd1 (+)	Ceppb (+)			
Irx3 (+)	Irx3 (+)			
Jun (+)	Jun (+)		Jun (+)	
Stat2 (+)		Stat2 (+)	Stat2 (+)	
	Nfkb1 (+)			**Nfkb1 (+)**
	Ddit3 (+)			Ppard(+)
	Junb (+)	Junb (+)		

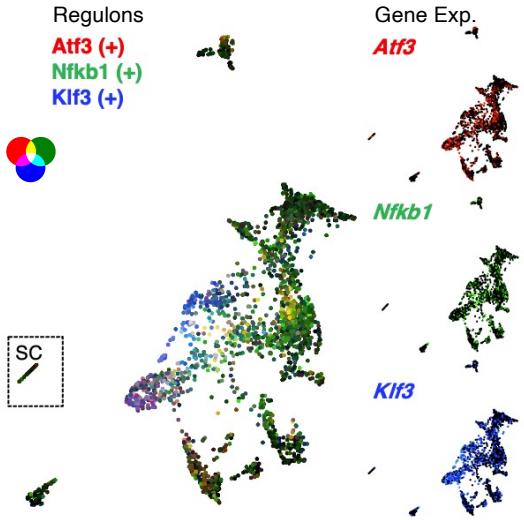

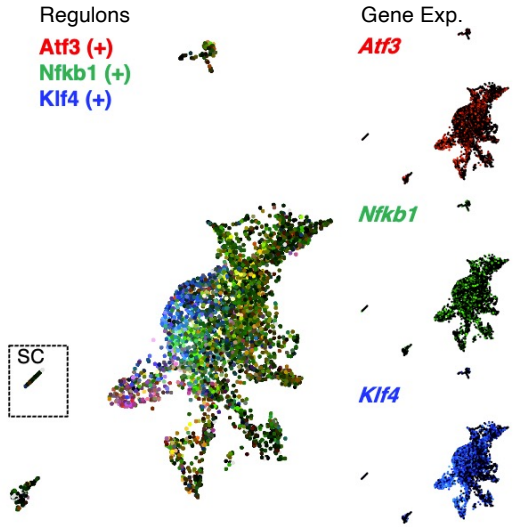

FIGURE 6

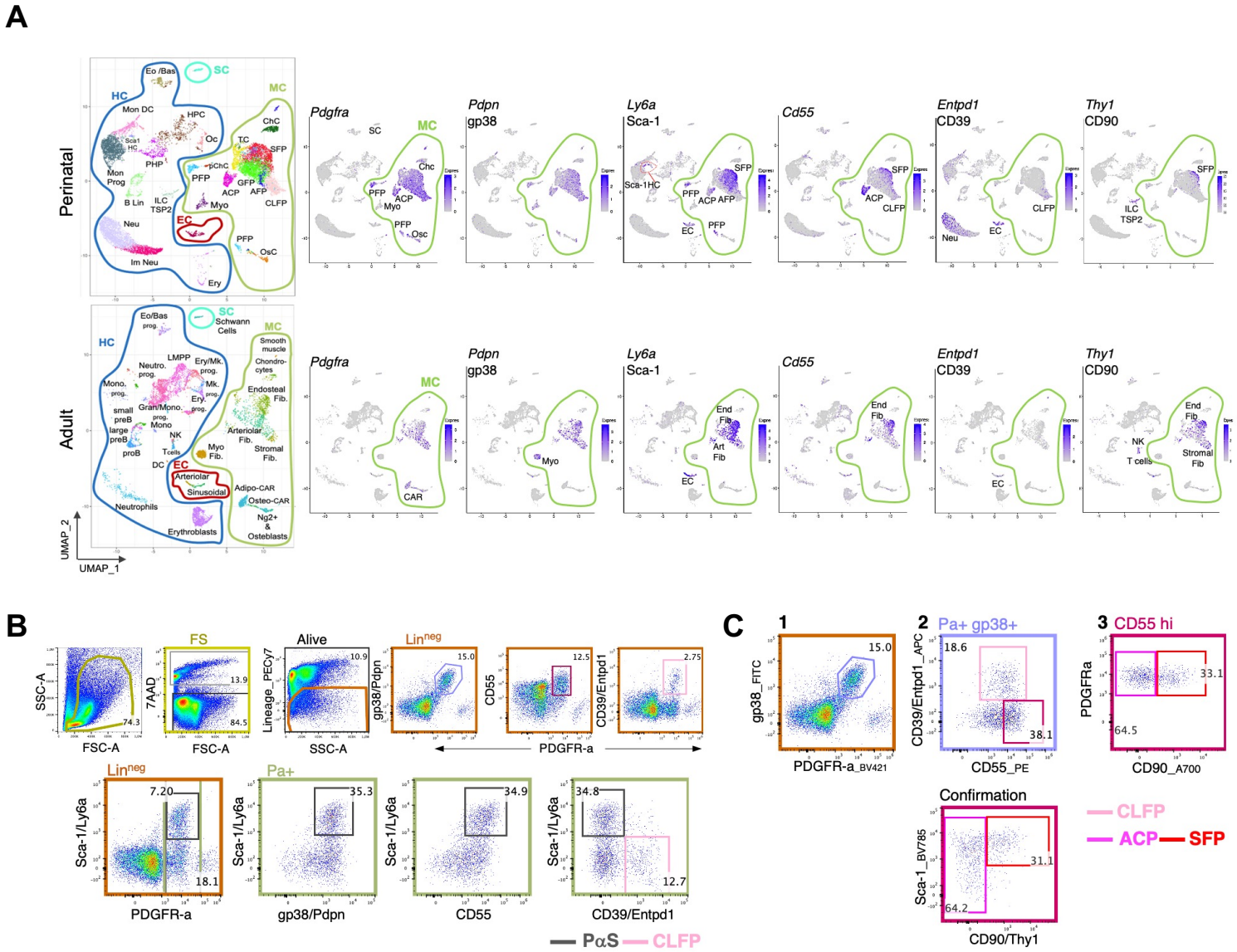
A
Perinatal
Adult
Pdgfra
Pdpn
gp38
Ly6a
Sca-1
Cd55
Entpd1
CD39
Thy1
CD90
UMAP_1
UMAP_2
B
FS
Alive
Lin^neg
Pa+
SSC-A
FSC-A
7AAD
Lineage_PECy7
gp38/Pdpn
CD55
CD39/Entpd1
PDGFR-a
Sca-1/Ly6a
PαS
CLFP
C
1
2 Pa+ gp38+
3 CD55 hi
gp38_FITC
PDGFR-a_BV421
CD39/Entpd1_APC
CD55_PE
PDGFRa
CD90_A700
Confirmation
Sca-1_BV785
CD90/Thy1
CLFP
ACP
SFP